Results in Engineering 27 (2025) 105809

Contents lists available at ScienceDirect

Results in Engineering

journal homepage: www.sciencedirect.com/journal/results-in-engineering

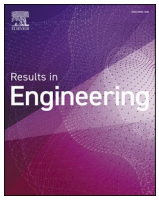

Research paper

A novel method for evaluation of the maintenance impact in the health of industrial components

F. Javier Bellido-Lopez [a,*], Miguel A. Sanz-Bobi [a], Antonio Muñoz [a], Daniel Gonzalez-Calvo [b], Tomas Alvarez-Tejedor [b]

[a] Institute for Research in Technology, ICAI School of Engineering, Pontifical Comillas University, Rey Francisco 4, Madrid 28015, Spain
[b] Enel Green Power and Thermal Generation, Endesa - Gas Maintenance Iberia, Ribera del Loira 60, Madrid 28042, Spain

ARTICLE INFO

Keywords:
Maintenance effectiveness
Failure indicator
Predictive maintenance
PHM
RCM

ABSTRACT

This study presents a novel method for evaluating maintenance effectiveness in industrial systems, built around the concept of "risk curves" as quantitative indicators of failure. By integrating Failure Mode and Effect Analysis (FMEA) with machine learning-based anomaly detection models, the proposed approach constructs risk curves by aggregating normalized deviations from monitored variables. These curves reflect the progression of failure modes in real time and enable a quantitative and accurate assessment of the impact of maintenance actions.

A key contribution of this research is the use of risk curves as an innovative method to continuously track the potential emergence of failure modes and quantify how maintenance actions contribute to reducing their associated risk. Applied to a feedwater pump in a combined-cycle power plant, these curves successfully detected critical failures, such as bearing wear and leaks, months in advance of traditional methods. Moreover, they provided a data-driven means to assess the effectiveness of maintenance actions, demonstrating their role as a determinant factor in improving component condition and mitigating failure risk.

The findings highlight the potential of this methodology to enhance maintenance strategies, reduce downtime, and foster improved collaboration between operation and maintenance teams. This research represents a significant advancement in maintenance evaluation, offering a scalable and data-driven framework that bridges existing gaps in failure diagnostics and decision-making processes.

1. Introduction

Industrial maintenance is a critical aspect of equipment and systems operation and management across various industries [1]. Over the years, maintenance strategies have evolved significantly. Initially, approaches were reactive, focusing on repairing failures only after they occurred [2]. Later, preventive approaches were introduced, designed to avoid failures through scheduled maintenance actions based on time intervals or specific operating conditions [3]. More recently, proactive approaches such as condition-based maintenance (CBM) and predictive maintenance (PdM) have further transformed the field by offering data-driven solutions to anticipate failures and optimize maintenance actions [4–6].

The advent of artificial intelligence (AI) has further accelerated this evolution, enabling sophisticated diagnostic and predictive capabilities in maintenance [7]. AI-driven methods, including machine learning-based models, enhance equipment health monitoring by using real-time data and advanced analytics to anticipate failures, thus improving operational efficiency and system reliability [4,8,9].

Effective maintenance is essential to ensure operational continuity, personnel safety, and resource optimisation, leading to increased competitiveness and operational efficiency [10,11]. As technologies advance, managing industrial equipment becomes more challenging, especially in complex systems where high performance and longevity are critical [12,13].

Traditionally, research in industrial maintenance has focused on early fault detection [14–16] and remaining useful life (RUL) prediction [17–19] to optimize maintenance actions. A wide range of anomaly detection techniques have been developed, including signal-based methods [20,21], dimensionality reduction [22,23], statistical models [24,25], and machine learning classifiers [26–28]. While these approaches are effective in detecting and classifying anomalies based on signal patterns or learned behaviours, they are typically disconnected from the maintenance process, and do not incorporate continuous

* Corresponding author.
E-mail address: jbellido@comillas.edu (F.J. Bellido-Lopez).

https://doi.org/10.1016/j.rineng.2025.105809
Received 21 February 2025; Received in revised form 6 June 2025; Accepted 16 June 2025
Available online 17 June 2025

indicators that link anomaly detection with maintenance evaluation.

Similarly, risk assessment is often based on traditional frameworks such as Failure Mode and Effect Analysis (FMEA) or Failure Mode, Effect, and Criticality Analysis (FMECA), which rely on fixed severity and detection scores assigned through expert judgment [29,30]. These methods are typically static, qualitative, and only weakly connected to real-time equipment condition or actual operational data. Although recent works have attempted to introduce more dynamic or data-driven formulations [31–33] these approaches remain limited in practice and rarely succeed in integrating risk evaluation with anomaly detection or the maintenance process itself.

The evaluation of maintenance effectiveness, particularly under the lens of the concept of "imperfect maintenance" [34], has become a pivotal concern [35,36], especially in contemporary industrial environments [21,37–39]. However, most contributions to date have been developed in the context of infrastructure systems, especially pavement management [40], where data availability and standardization are more advanced [41,40,42,43]. In contrast, maintenance effectiveness remains underexplored in general industrial applications, often due to the lack of high-quality data for non-infrastructure assets [44–46]. Furthermore, many proposed methods lack quantitative formulation or validation in real-world settings [21,40,47,48], and are typically designed for isolated case studies. Most importantly, there is still a lack of integrated approaches capable of connecting real-time condition monitoring with the evaluation of maintenance impact [49].

This work addresses these gaps by proposing a unified methodology that combines residual-based anomaly detection with dynamic risk curve modelling, enabling a continuous and quantitative evaluation of maintenance effectiveness. While industrial operators typically rely on SCADA systems or similar platforms to monitor real-time performance, maintenance teams often lack an equivalent tool to track equipment degradation or assess the true impact of their maintenance actions. The proposed method fills this gap by constructing a real-time failure indicator, the risk curve, that supports continuous monitoring and maintenance evaluation, bridging the disconnect between condition monitoring and maintenance strategy.

Incorporating this method addresses long-standing challenges in maintenance assessment and opens new opportunities for improving industrial processes. Beyond its technical contributions, the methodology enhances collaboration and communication between operations and maintenance teams by providing shared, quantitative indicators of equipment health and the results of maintenance actions. Ultimately, this approach supports data-driven decision-making, optimizes maintenance strategies, reduces costs, and improves both system reliability and operational efficiency.

The main contributions of this paper are:

- The development of a unified, data-driven framework that integrates anomaly detection, risk modelling, and maintenance evaluation into a continuous decision-support tool.
- The introduction of the risk curve, a novel real-time indicator that quantifies failure risk evolution and enables the post-intervention evaluation of maintenance actions.
- The proposal of a methodology capable of quantifying the reduction in risk level associated with specific failure modes, offering a precise and continuous measure of maintenance effectiveness.
- A contribution to sustainable and informed maintenance management by enhancing coordination between operations and maintenance through actionable, real-time insights.

The remainder of the paper is structured as follows: Section 2 details the proposed method, including failure mode analysis, model design, risk curve construction, and maintenance effectiveness evaluation. Section 3 presents a real-world case study on a feedwater pump in a combined-cycle power plant, discussing the results in detail and addressing the practical challenges encountered during implementation. Section 4 discusses the findings, conclusions, and future research directions.

2. Methodology

The proposed methodology evaluates the impact of maintenance actions on equipment health, with a central focus on developing a reliable anomaly detection method. In this manner, the methodology follows a logical sequence of interconnected steps aimed at creating a failure indicator, which represents the risk of failure occurrence.

Firstly, the identification of potential failure modes through Failure Mode and Effect Analysis (FMEA) establishes the basis for defining and developing data-driven predictive models for anomaly detection.

Once the models are defined, they are trained to characterize the expected normal behaviour of the equipment for any normal operating condition (NOC). This phase establishes a baseline for the identification of anomalies. By monitoring the current state of the equipment and comparing it to this baseline, significant deviations can be detected, indicating the emergence of potential failures.

These deviations are used to build the failure indicator, known as the risk curve. These curves dynamically quantify the risk of occurrence and relative severity of potential failure modes over time and allow the condition of the equipment to be diagnosed in real time.

The final step is to evaluate the effectiveness of the maintenance actions: the profile of the failure indicator is analysed before and after the actions, quantifying their impact, i.e. their effectiveness. This comprehensive process, based on equipment condition and failure mechanisms, verifies that maintenance actions were applied and supports the transition from reactive to predictive maintenance strategies.

Fig. 1 illustrates the logical flow of the proposed methodology, highlighting the connections between its components. Each step builds upon the outputs of the preceding one, ensuring a cohesive and robust framework for maintenance evaluation. The methodology is explained in detail, step-by-step, in the following sections.

This methodological framework represents a significant contribution in current practices of risk evaluation of possible failure modes by explicitly incorporating maintenance effectiveness as a measurable outcome. In contrast to traditional approaches that often focus exclusively on detection or diagnosis, this unified process enables a comprehensive evaluation of maintenance impact, positioning it as a valuable tool for optimising maintenance strategies and improving asset reliability.

2.1. Failure Mode and Effect Analysis (FMEA) and models' definition

The first step is to perform a FMEA of the equipment under analysis [50,51]. It involves identifying all potential failures that could occur in the equipment (FM_i, $i = 1, 2, \ldots, m$, where m is the number of failure modes identified), along with their effects, severity, and potential detection methods. In order to determine the possible detection methods, it is first necessary to identify the monitored variables of the equipment (X_j, $j = 1, 2, \ldots, p$, where p is the number of monitored variables). This enables the creation of a relational map between these variables and the failure modes (Fig. 2).

Unlike traditional FMEA approaches that use numerical scoring for severity, occurrence, and detectability to prioritize failure modes, our methodology focuses on defining data-driven detection models for all relevant failure modes, rather than ranking them. The relationships between monitored variables and failure modes are defined qualitatively, using expert knowledge and operational relevance. This approach avoids subjectivity in scoring and enables failure risk to be evaluated dynamically through the evolution of risk curves. Although a more detailed criticality assessment, such as a Failure Mode, Effect, and Criticality Analysis (FMECA), could be considered in future developments, our current goal is to monitor the behaviour of each failure mode in real time and assess the impact of maintenance actions.

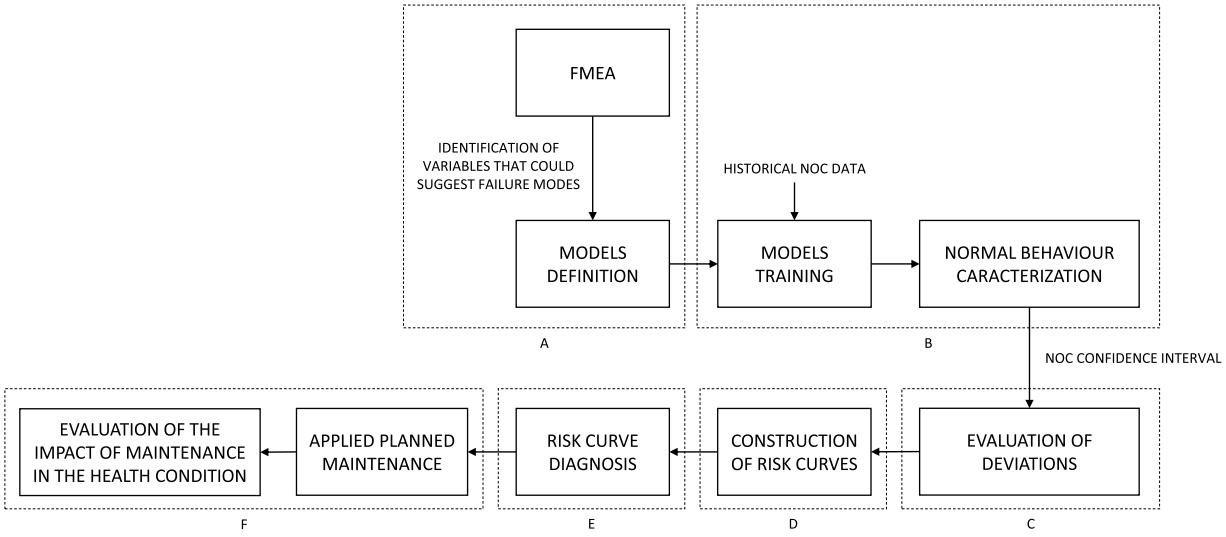

Fig. 1. Block diagram of the proposed method.

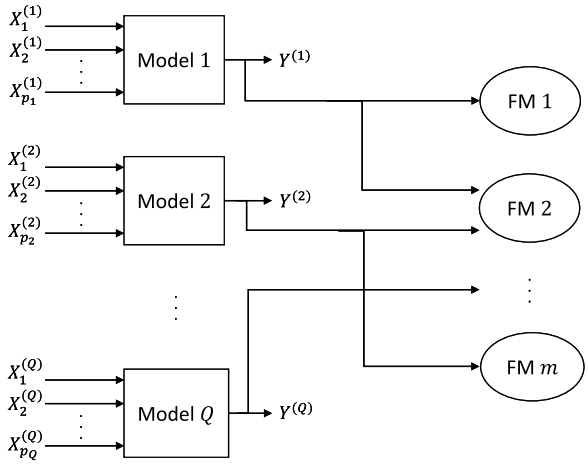

Fig. 2. Block diagram of model definition based on FMEA.

The integration of this map with expert knowledge facilitates the definition of the models required to monitor the occurrence of each failure mode. Specifically, it defines the output variables of the models (Y_k, $k = 1,\ 2,\ \ldots,\ Q \geq m$, where Q is the number of defined models and $Y_k \in \{X\}$). Depending on the detection method, models may share output variables, multiple models may correspond to a single failure mode, or a single model may cover several failure modes.

The input variables of each model [$X_s^{(k)}$, $k \in [1,\ Q]$, $s = 1,\ 2,\ \ldots,\ p_k < p$, where X_s is the s-th input variable, k is the model number and p_k is the number of input variables of the model k] are selected from all the monitored variables ($X_s^k \in \{X\}$) based on the physics of the problem to be detected and the relationships between variables.

2.2. Model training and obtention of the NOC residual range

Once the Q models have been defined, historical data of normal operating conditions of the equipment, $\{X\}_{\text{NOC}}$, are collected and used to train the models.

Normal operating conditions (NOC) are defined as the set of time intervals during which the equipment operates within its specified normal operating ranges, as established in the manufacturer's operating/maintenance manual, without the occurrence of failures and major maintenance actions. Transient regimes, such as start-up and shutdown phases, are excluded from this definition. The NOC set includes all operational modes of the equipment, ensuring that the behaviour across different steady-state regimes is represented. In addition, anomalous or isolated outliers that may distort the normal behaviour baseline are also discarded.

In this manner, the models, when confronted with new values of their input variables, $\{X^{(k)}\}_{\text{new}}$, will provide the expected value of the variable monitored by the equipment under normal operating conditions, $Y_{\text{NOC}}^{(k)}$. For this reason, these models are typically designated as NOC models. Consequently, the set of models is capable of simulating the expected normal behaviour of the equipment.

This approach is consistent with the fundamental principles of analytical redundancy relations (ARRs), which have been extensively utilised in the domain of fault detection and isolation for dynamic systems [52]. ARRs exploit the redundancy inherent in system equations to detect inconsistencies between observed and expected behaviour, a concept that provides the foundation for model-based fault detection methods.

To quantitatively monitor the real behaviour of the equipment, a comparison is made between the real value of the variables and the expected value. In other words, the variables are monitored in terms of the deviations between their actual and simulated values, $E^{(k)}$:

$$E^{(k)}(t) = Y^{(k)}(t) - Y_{\text{NOC}}^{(k)}(t) \tag{1}$$

where t is the time variable indicating the sample being analysed.

Therefore, to utilise these differences as a source of valuable insight, it is essential to characterise the normal behaviour of the models' output variables by analysing their residuals, $\{E^{(k)}\}_{\text{NOC}}$. This is achieved by fitting the distribution function of the residuals obtained in model training, $P(E^{(k)})$, and defining a confidence interval for normal behaviour:

$$\text{CI}_{\text{NOC}}^{(k)} = \left[L_{inf}^{(k)},\ L_{sup}^{(k)}\right] \tag{2}$$

from this distribution. In other words, when a new value of the output variable for one of the models is received, the difference between this value and the simulated value, the residual, is calculated. If the residual falls within the confidence interval, it can be concluded that the variable is behaving as expected:

$$\begin{aligned} &E^{(k)}(t) = Y^{(k)}(t) - Y_{\text{NOC}}^{(k)}(t) \\ &E^{(k)}(t) \in \text{CI}_{\text{NOC}}^{(k)} \rightarrow Y^{(k)}(t) \text{ is behaving normally} \end{aligned} \tag{3}$$

This methodology is rooted in model-based fault detection, a well-established field that has been extensively reviewed by [53]. A notable advantage of this approach is that it does not require the existence of a history of failure data to train models capable of identifying the patterns that characterise them. This is a common challenge in conventional classification methods employed for fault detection and diagnosis [54–56]. Instead, the objective here is to train regression models that generalize normal behaviour using only a sufficiently large dataset. Since the real values under normal operating conditions serve as the labels, supervised learning ML algorithms can be applied in a straightforward and reliable manner.

2.3. Detection of significant deviations

Conversely, if the residual falls outside the specified confidence interval, it can be inferred that the value of the variable is anomalous:

$$E^{(k)}(t) \notin \mathrm{CI}_{\mathrm{NOC}}^{(k)} \rightarrow Y^{(k)}(t) \text{ is anomalous} \tag{4}$$

When C or more consecutive anomalous values are detected, the variable is classified as deviating from normal behaviour. Consequently, the associated failure mode may be considered at increasing risk: either developing, imminent, or possibly already occurred.

The decision to designate a threshold value of C outliers is informed by accumulated experience. When fewer than C anomalous values are detected, they are treated as noise, false positives, or sporadic deviations and excluded from the analysis. This reflects the assumption that true failures affect equipment behaviour persistently over time, rather than resolving spontaneously.

The parameter C is adjustable and depends on the characteristics of each application. Lower values increase sensitivity to transient deviations but may lead to higher false positive rates due to sensor noise, while higher values provide greater robustness against noise but may delay failure detection. The choice of C, therefore, represents a trade-off between early detection and detection reliability.

According to (3) and (4), the deviations are calculated as one plus the absolute value of the distance of the residual obtained to the extreme of the confidence interval of the same sign divided by the value of this extreme:

$$\begin{cases} \mathrm{DEV}^{(k)}(t) = 1 + \dfrac{\left|E^{(k)}(t) - L_{inf}^{(k)}\right|}{\left|L_{inf}^{(k)}\right|} \text{ if } E^{(k)}(t) < L_{inf}^{(k)} \\ \mathrm{DEV}^{(k)}(t) = 0 \text{ if } E^{(k)} \in \left[L_{inf}^{(k)},\ L_{sup}^{(k)}\right] \\ \mathrm{DEV}^{(k)}(t) = 1 + \dfrac{\left|E^{(k)}(t) - L_{sup}^{(k)}\right|}{\left|L_{sup}^{(k)}\right|} \text{ if } E^{(k)}(t) > L_{sup}^{(k)} \end{cases} \tag{5}$$

The value of one is assigned to mark the threshold where the residual just exceeds the confidence interval limit and is considered a deviation. Dividing by the confidence interval limit normalizes the deviation, ensuring comparability across models.

2.4. Construction of risk curves

The concept of risk curve plays a pivotal role in the proposed methodology, since they constitute the proposed failure indicator. The construction of these curves involves the generation of risk curves for the previous NOC models. For each of these models, the risk curve, $f(t)$, is created by calculating the cumulative sum of normalized deviations detected over time. By aggregating these normalized deviations over time, the risk curve captures the evolution and persistence of anomalies in the equipment's behaviour:

$$f^{(k)}(t) = \sum_{n=t_0}^{t} \mathrm{DEV}^{(k)}(n) \tag{6}$$

where t_0 is the reference time, i.e. the time corresponding to the first available sample.

Given that a single failure mode may exert influence on multiple operating variables, the risk curve for a given failure mode is derived as a weighted sum of the risk curves from the relevant NOC models. The weights reflect the relative importance of each model's output variable in monitoring the specific failure mode.

Determined in consultation with experts, these weights leverage operational knowledge to prioritize critical variables based on the understanding of failure mechanisms and their observable symptoms. In addition, the weighting scheme could also incorporate empirical information such as the historical frequency of deviations observed in each monitored variable, which may evolve over time as more operational data becomes available. This would allow the weights to progressively reflect both expert knowledge and system behaviour throughout its operational life.

To maintain consistency, the weights are normalized such that their sum equals one, effectively assigning a proportional influence to each model:

$$f^{(i)}(t) = \sum_{k} \omega_k f^{(k)}(t) \tag{7}$$

$$\sum_{k} \omega_k = 1 \tag{8}$$

where i is the failure mode under consideration, k runs through the NOC models used to monitor it and $\omega_k > 0$.

Fig. 3 provides an overall visual summary of the methodology, illustrating the entire process: from data acquisition and residual calculation, through the construction and aggregation of risk curves, to the evaluation of maintenance effectiveness. This diagram complements the equations and procedures described in Sections 2.2–2.4 and shows how these steps connect to the evaluation stages in Sections 2.5 and 2.6, forming a continuous monitoring and decision-support framework.

*Note: The graphical elements marked with an asterisk (*) refer to illustrative outputs that will be presented and discussed in detail in the case study (Section 3, Figs. 13, 14, 16 and, 18). **

2.5. Risk curve diagnosis

As the term implies, risk curves are utilised to quantify the proximity of a specific failure mode occurring: the higher the risk, the closer and more likely the failure is to occur. Since the measure of risk, as mentioned above, is relative, the maximum risk threshold for each failure mode is determined based on historical cases of failure. In other words, the risk curve of the past is constructed and the level of risk that existed when the failure mode occurred is determined. This risk value can then be used as the maximum threshold for future events, $f_{\max}^{(i)}$, indicating that, based on the past, the failure mode has occurred.

In the event of multiple historical failure cases being identified with different maximum risk levels, the lowest level should be selected, as this ensures a more conservative assessment of the risk, thereby avoiding the overestimation of the criticality of the failure mode.

Even without historical failure data for the considered failure mode, the risk curve remains useful. Qualitatively, it shows how failure risk evolves over time. And quantitatively, it serves as the indicator to evaluate maintenance effectiveness, as described in the following section.

Therefore, once the risk curves for all the failure modes to be monitored have been constructed, it is sufficient to analyse two aspects: (1) the level of risk associated with each failure mode and its proximity

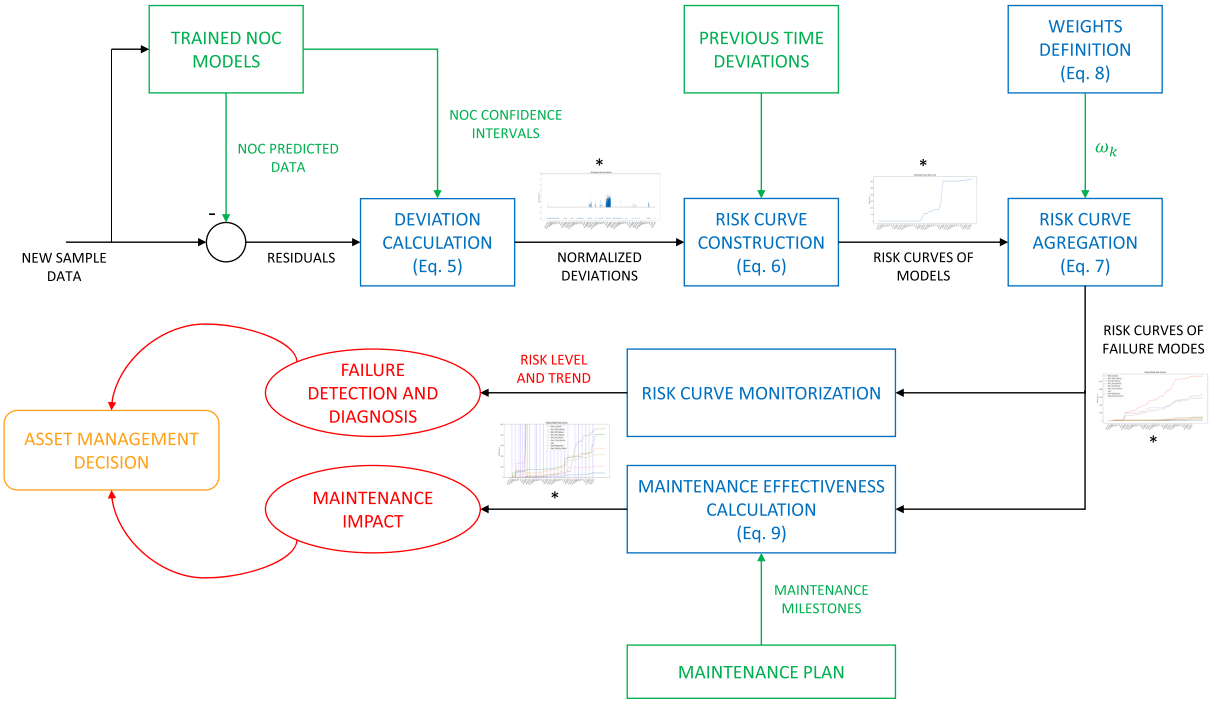

Fig. 3. Detailed flowchart of the proposed methodology.

to the maximum threshold, since this indicates the risk of occurrence, $|f^{(i)}_{\max} - f^{(i)}(t)|$, and (2) the slope of the curve between two samples t_1 and t_2 ($t_2 > t_1$), $\Delta f^{(i)}(t)/\Delta t|_{t_1}^{t_2}$, which indicates how quickly and sharply the risk evolves and provides insight into the severity of the failure mode detected.

If the slope of a risk curve is zero, it indicates that, with respect to the corresponding failure mode, the equipment has returned to normal behaviour. Furthermore, although the risk has increased, if it is far from the maximum threshold, there is still room for some maintenance action, if it is considered necessary. Conversely, if the slope is consistently positive, indicating an ongoing increase in risk, it is likely that the equipment has sustained some form of damage affecting the corresponding failure mode. This necessitates prompt maintenance action.

$$\begin{cases} \Delta f^{(i)}(t)\Big/\Delta t\Big|_{t_1}^{t_2} = 0 \rightarrow \text{Normal behaviour} \\ \Delta f^{(i)}(t)\Big/\Delta t\Big|_{t_1}^{t_2} > 0 \rightarrow \text{Failure mode in progress} \end{cases}$$

2.6. Maintenance impact evaluation

Finally, risk curves are an invaluable tool for assessing the effectiveness of a maintenance action, since they are failure indicators. Essentially, the impact of a maintenance action, a, can be quantified by comparing the failure indicator, i.e. the risk curve, of the failure mode k that is intended to be affected before, $t_{\text{bef}} < t_a$, and after $t_{\text{aft}} > t_a$ the action has been performed:

$$\text{ef}_a = 1 - \frac{\Delta f^k/\Delta t|_{t_a}^{t_{\text{aft}}}}{\Delta f^k/\Delta t|_{t_{\text{bef}}}^{t_a}} \tag{9}$$

where t_a is the time corresponding to the maintenance action.

Three cases can be distinguished:

- If the calculated effectiveness is positive, it indicates that, after the maintenance action, the risk of the considered failure mode is growing more slowly than before, or has even stopped increasing entirely ($\text{ef}_a = 1$). In this case, the maintenance action was effective, and the degree of effectiveness is given by the calculated value.
- If the effectiveness is zero, the risk continues to grow at the same rate as before, indicating that the maintenance action had no impact on the failure mode.
- If the effectiveness is negative, the risk grows faster after the action than before, meaning the maintenance action not only failed to solve the problem but worsened the situation.

This evaluation allows the effectiveness of different maintenance actions to be assessed, identifying which actions are beneficial for each failure mode and to what extent.

3. Case study of the proposed method

In this section, the method proposed in the previous section is applied step by step to a real industrial installation: a feedwater pump within the water-steam circuit of a combined-cycle power plant. The data used in this process are real operational data obtained directly from the plant's control room.

Fig. 4 illustrates the location and function of the feedwater pump within the overall layout of a combined-cycle power plant. The pump is positioned in the water-steam circuit, downstream from the condenser and upstream of the heat recovery steam generator (HRSG). Its role is to pressurize and deliver high-pressure water to the HRSG, enabling the generation of high-pressure steam that feeds the steam turbine. Given its position, the pump is a critical component for the continuity and efficiency of the steam cycle, and any failure in its operation can lead to a shutdown or significant derating of the plant. This functional relevance, combined with the availability of monitoring data, makes the feedwater pump an ideal candidate for illustrating the proposed methodology.

3.1. Failure Mode and Effect Analysis (FMEA) and models' definition

In developing the FMEA, $m = 9$ potential failure modes that may occur in the pump were considered [51]:

- Motor overload (FM_1).

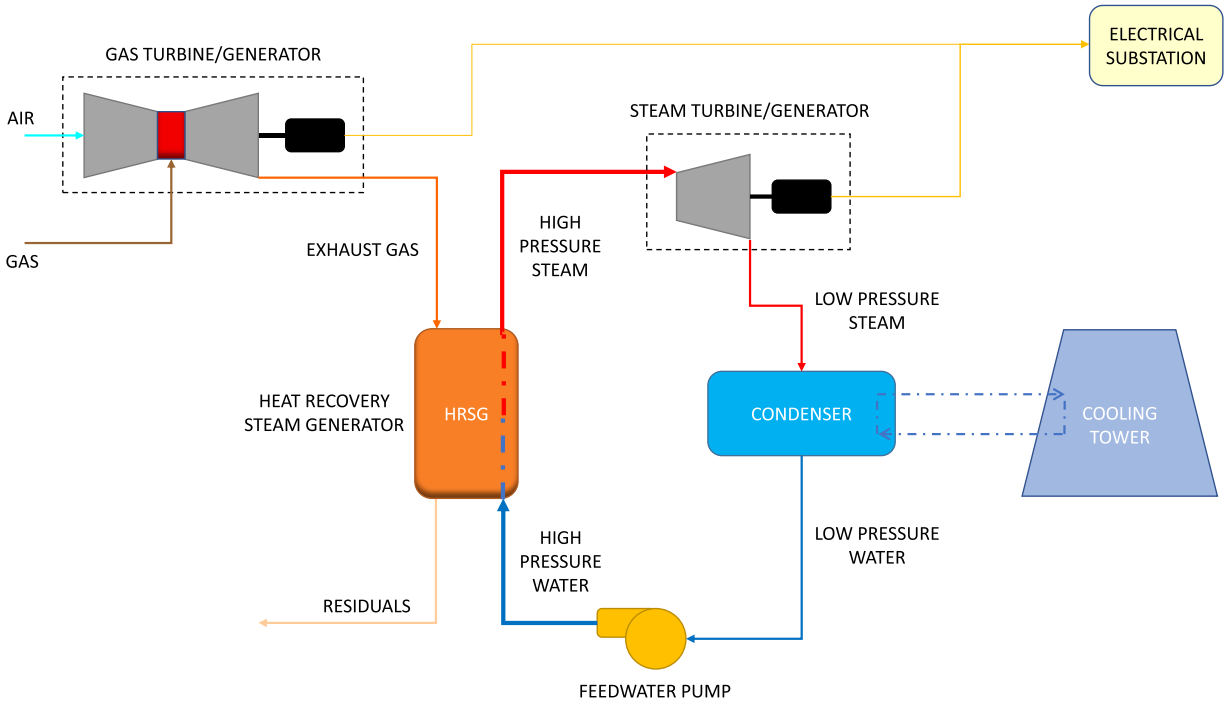

Fig. 4. Simplified schematic of a combined-cycle power plant.

- Worn opposite motor coupling side (OMCS) bearing (FM_2).
- Worn motor coupling side (MCS) bearing (FM_3).
- Worn opposite side of the pump coupling (OPCS) bearing (FM_4).
- Worn pump coupling side (PCS) bearing (FM_5).
- Worn thrust bearing (FM_6).
- Leak (FM_7).
- Shaft misaligned (FM_8).
- Motor electrical failure (FM_9).

And the data permit access to $p = 25$ monitored variables, the description and unit of measurement are presented in Appendix B (Table 7). The list of variables is as follows:

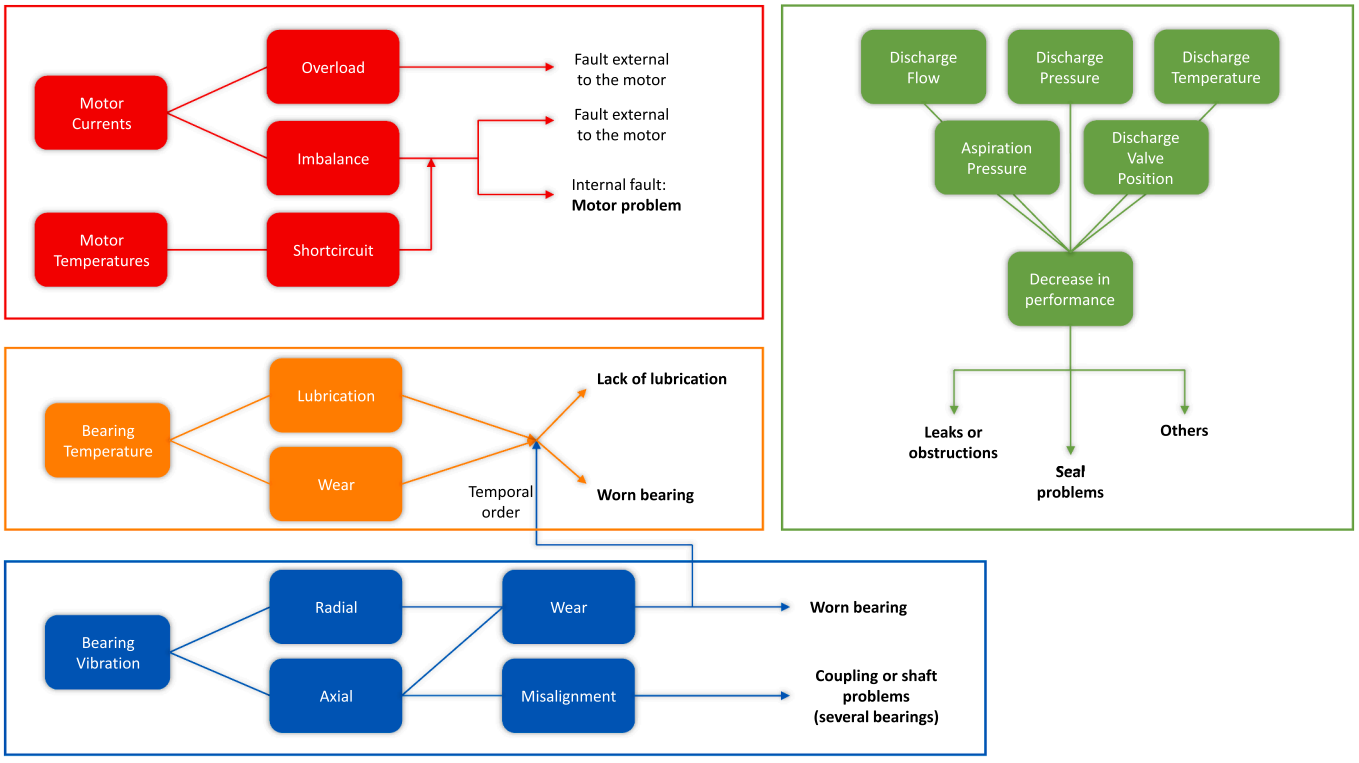

Fig. 5. Relational map of failure modes and monitored variables based on FMEA.

- Motor phase R current (X_1), motor phase S current (X_2), motor phase T current (X_3), motor phase R temperature (X_4), motor phase S temperature (X_5) and motor phase T temperature (X_6).
- Average motor current (X_7).
- Temperature of the 5 p.m. and motor bearings: OMCS bear temperature (X_8), MCS bear temperature (X_9), OPCS bear temperature (X_{10}), PCS bear temperature (X_{11}) and thrust bear temperature (X_{12}).
- Vibrations of three of the pump bearings: thrust bearing vibration (X_{13}), PCS bearing displacement in direction 1 (X_{14}), PCS bearing displacement in direction 2 (X_{15}), OPCS bearing displacement in direction 1 (X_{16}), OPCS bearing displacement in direction 2 (X_{17}).
- Discharge valve position (X_{18}).
- Aspiration pressure (X_{19}).
- Discharge pressure (X_{20}), flow rate (X_{21}), and temperature (X_{22}).
- Power of the gas turbine (X_{23}) and steam turbine (X_{24}) associated with the pump.
- Operation mode (X_{25}).

As previously mentioned, this study leverages FMEA as a starting point to identify potential relationships between observable variables and possible failure modes. A detailed FMEA table, including the identified failure modes, their effects, and the monitored variables associated with each one, is provided in Appendix A (Table 6). Fig. 5 illustrates the relational map constructed based on this approach.

As explained in Section 2, this map facilitates the identification of which variables allow the detection of which failure modes, and therefore the definition of the NOC models needed for anomaly detection. Considering the monitored variables, the $Q = 23$ selected NOC models are defined in Tables 1, and 2 determines the relationship between the failure modes and each of the models. As is observable, a single model may be utilised to monitor multiple failure modes, and a single failure mode may necessitate the employment of more than one model for its detection.

In order to illustrate the step-by-step development of the method, one of the models will be chosen as an example. However, it should be noted that the procedure is identical for the remaining models. The model selected is the "Discharge Flow Model" (Fig. 6), which predicts the normal behaviour of discharge flow rate. This model is employed for the purpose of monitoring potential failure modes, including water leaks. The model's input variables, consulting Table 1, are the average current of the motor driving the pump and the power of the gas turbine associated with the pump's boiler:

3.2. Model training and obtention of the NOC residual range

The primary objective of NOC models is to predict the normal behaviour of their output variable, in this case, the pump discharge flow rate, under steady state conditions. Since these are data-driven models, they require a training dataset that characterises the normal behaviour of the equipment.

As defined in Section 2.2, normal operating conditions (NOC) correspond to time intervals in which the equipment operates within its prescribed operating ranges, without incidents or maintenance actions, and excluding transients. For this case study, NOC intervals were identified using the operational boundaries established by the Electric Power Research Institute (EPRI) Maintenance Guideline [57], in conjunction with maintenance records from the plant. These intervals include all steady-state operational modes of the pump and were validated by the plant's maintenance team.

Based on this definition and validation process, the dataset employed in this study, X (see Section 2.1), spans a four-year period from December 2019 to December 2023, with 10-min sampling intervals. After filtering for steady-state operation, the final dataset includes over 125,000 valid samples for each one of the 25 monitored variables, plus the corresponding time array. This data was provided by the Spanish company ENDESA. However, it should be noted that the data, collected directly from one of its operational power plants, is classified as confidential due to the sensitive nature of the company's operations.

Fig. 7 illustrates the discharge flow rate data that has been collected (the gaps with no data are due to periods when the pump was not operating). Utilising the maintenance information provided by the

Table 1
NOC models' definition.

Model	Output variable (Y_k)	Input variables
M_1	Discharge flow rate	Average motor current Gas turbine power
M_2	Phase R current	Phase S current Phase T current
M_3	Phase S current	Phase R current Phase T current
M_4	Phase T current	Phase R current Phase S current
M_5	Phase R temp.	Phase S temp. Phase T temp.
M_6	Phase S temp.	Phase R temp. Phase T temp.
M_7	Phase T temp.	Phase R temp. Phase S temp.
M_8	Phase R current	Steam turbine power Gas turbine power Operation mode
M_9	Phase S current	Steam turbine power Gas turbine power Operation mode
M_{10}	Phase T current	Steam turbine power Gas turbine power Operation mode
M_{11}	Phase R temp.	Aspiration pressure Steam turbine power Gas turbine power
M_{12}	Phase S temp.	Aspiration pressure Steam turbine power Gas turbine power
M_{13}	Phase T temp.	Aspiration pressure Steam turbine power Gas turbine power
M_{14}	PCS bear disp. Dir1	Aspiration pressure Steam turbine power Gas turbine power
M_{15}	PCS bear disp. Dir2	Aspiration pressure Steam turbine power Gas turbine power
M_{16}	OPCS bear disp. Dir1	Aspiration pressure Steam turbine power Gas turbine power
M_{17}	OPCS bear disp. Dir2	Aspiration pressure Steam turbine power Gas turbine power
M_{18}	Thrust bear vibration	Thrust bearing temp. Aspiration pressure Steam turbine power Gas turbine power
M_{19}	PCS bear temp.	Phase R temp. Aspiration pressure Steam turbine power Gas turbine power
M_{20}	OPCS bear temp.	Phase R temp. Aspiration pressure Steam turbine power Gas turbine power
M_{21}	MCS bear temp.	Phase R temp. Aspiration pressure Steam turbine power Gas turbine power
M_{22}	OMCS bear temp.	Phase R temp. Aspiration pressure Steam turbine power Gas turbine power
M_{23}	Thrust bear temp.	Phase R temp. Aspiration pressure Steam turbine power Gas turbine power

Table 2
Relationship between NOC models and failure modes under monitoring.

Failure Mode	NOC Model
Motor overload (FM_1)	Phase R current (M_2)
	Phase S current (M_3)
	Phase T current (M_4)
	Phase R current (M_8)
	Phase S current (M_9)
	Phase T current (M_{10})
Worn OMCS bearing (FM_2)	OMCS bear temp. (M_{22})
Worn MCS bearing (FM_3)	MCS bear temp. (M_{21})
Worn OPCS bearing (FM_4)	OPCS bear disp. Dir1 (M_{16})
	OPCS bear disp. Dir2 (M_{17})
	OPCS bear temp. (M_{20})
Worn PCS bearing (FM_5)	PCS bear disp. Dir1 (M_{14})
	PCS bear disp. Dir2 (M_{15})
	PCS bear temp. (M_{19})
Worn thrust bearing (FM_6)	Thrust bear vibration (M_{18})
	Thrust bear temp. (M_{23})
Leak (FM_7)	Discharge flow rate (M_1)
	Phase R current (M_8)
	Phase S current (M_9)
	Phase T current (M_{10})
Shaft misaligned (FM_8)	PCS bear disp. Dir1 (M_{14})
	PCS bear disp. Dir2 (M_{15})
	OPCS bear disp. Dir1 (M_{16})
	OPCS bear disp. Dir2 (M_{17})
	Thrust bear vibration (M_{18})
	PCS bear temp. (M_{19})
	OPCS bear temp. (M_{20})
	MCS bear temp. (M_{21})
	OMCS bear temp. (M_{22})
	Thrust bear temp. (M_{23})
Motor electrical failure (FM_9)	Phase R current (M_2)
	Phase S current (M_3)
	Phase T current (M_4)
	Phase R temperature (M_5)
	Phase S temperature (M_6)
	Phase T temperature (M_7)
	Phase R current (M_8)
	Phase S current (M_9)
	Phase T current (M_{10})
	Phase R temperature (M_{11})
	Phase S temperature (M_{12})
	Phase T temperature (M_{13})

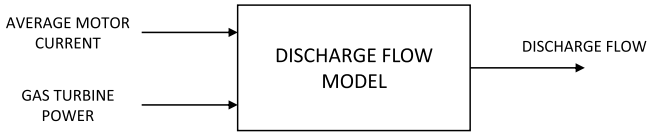

Fig. 6. Discharge flow model block diagram.

company, a representative period of normal behaviour has been determined, spanning from December 2019 to July 2020 (orange points in Fig. 8), which resulted in over 25,000 valid samples for each of the 25 monitored variables and the time array. This dataset was used to train and validate the NOC models. The remainder of the four-year dataset was used for testing and for applying the proposed methodology.

The supervised machine learning (ML) algorithm and its hyperparameters are selected through an iterative process that involves training the model multiple times with different configurations and algorithms. To this end, the results obtained are compared with those of common algorithms in many, such as linear regression (LR), k-Nearest Neighbour (kNN), decision tree (DT), support vector machine (SVM) and multi-layer perceptron (MLP) [58–61]. The metric used to evaluate performance is the root-mean-square error (RMSE), which is one of the most common for regression models.

In the particular case of the “Discharge Flow Model”, according to Table 3, the algorithm that offers the best results is the multi-layer perceptron (MLP). To optimise its hyperparameters, Optuna, an open-source Bayesian optimisation framework, was employed, enabling efficient exploration of the configuration space and identification of an optimal model configuration [62,63].

Once the optimal hyperparameters has been identified and applied, the model undergoes definitive training through the utilisation of cross-validation. To achieve this, the normal behaviour data is divided into two sets: one for training (80 %) and one for validation (20 %). Fig. 9 shows the model prediction for a section of the training data set once the model has been optimally trained.

The final hyperparameters of the discharge flow rate model, along with the obtained root-mean -squared error (RMSE) for the training and validation datasets, are outlined in Table 4. The configuration and performance of the other models analysed are presented in Appendix C (Tables 7–33).

As shown in Fig. 10, the residuals of the training dataset (see Eq. (1)), if the training process has been successful, should follow a distribution that is similar to a normal distribution with a mean of zero. This is due to the fact that data over a period of normal behaviour will fluctuate as if it were random noise around its average value.

As stated in Section 2, the objective of these models is to characterise the normal behaviour of their outputs. To this end, an analysis of the distribution of their training residuals is conducted, from which the confidence interval of the normal behaviour of the output variable residual is calculated (see Eq. (2)). The distribution of the training residuals is then adjusted using the Gaussian Mixture Model (GMM) technique (see Fig. 11), whose optimal components are selected based on the Bayes Information Criterion (BIC). According to the empirical rule of statistics (rule 68–95–99.7), a confidence interval of 99.7 % is selected (see Fig. 12).

3.3. Detection of significant deviations

Once the normal behaviour of the pump has been characterised by the confidence interval, it is used to detect possible significant deviations in the entire set of historical data. Fig. 13 illustrates significant deviations ($C = 3$) detected in the pump discharge flow rate, calculated from Eq. (5).

Several values of C were tested during the analysis. Lower thresholds ($C < 3$) resulted in excessive sensitivity to sensor noise and produced a higher number of false positives. Conversely, higher thresholds ($C > 3$) led to delays in failure detection, as sustained deviations needed to persist longer before being recognized. The value $C = 3$ was therefore selected as an appropriate balance between detection sensitivity and robustness to noise [64], consistent with the behaviour observed in this dataset.

3.4. Construction of risk curves

Using Eq. (6), the risk curve for the pump discharge flow rate is constructed (Fig. 14).

As stated in Section 2, the objective is to monitor the risk associated with each failure mode, rather than that of each model in particular. This is due to the fact that the same failure mode can be reflected in several variables of the equipment. Consequently, as delineated in Eq. (7), risk curves are constructed for each failure mode. Fig. 15 illustrates the relationship between failure modes and models, as outlined in Table 2, and the weights assigned to the models for each failure mode.

The weight assignment follows the same expert-driven criteria described in Section 2.4, reflecting the diagnostic relevance of each monitored variable to the failure mode under analysis.

To illustrate this, the "Leak" failure mode is taken as an example. According to the maintenance experts of the company that provided the data, the models involved in this failure mode are those that predict the discharge flow rate (Discharge Flow Model) and the currents of the pump motor phases (Current Phase R Model, Current Phase S Model, Current Phase T Model). The weights associated with each of the models

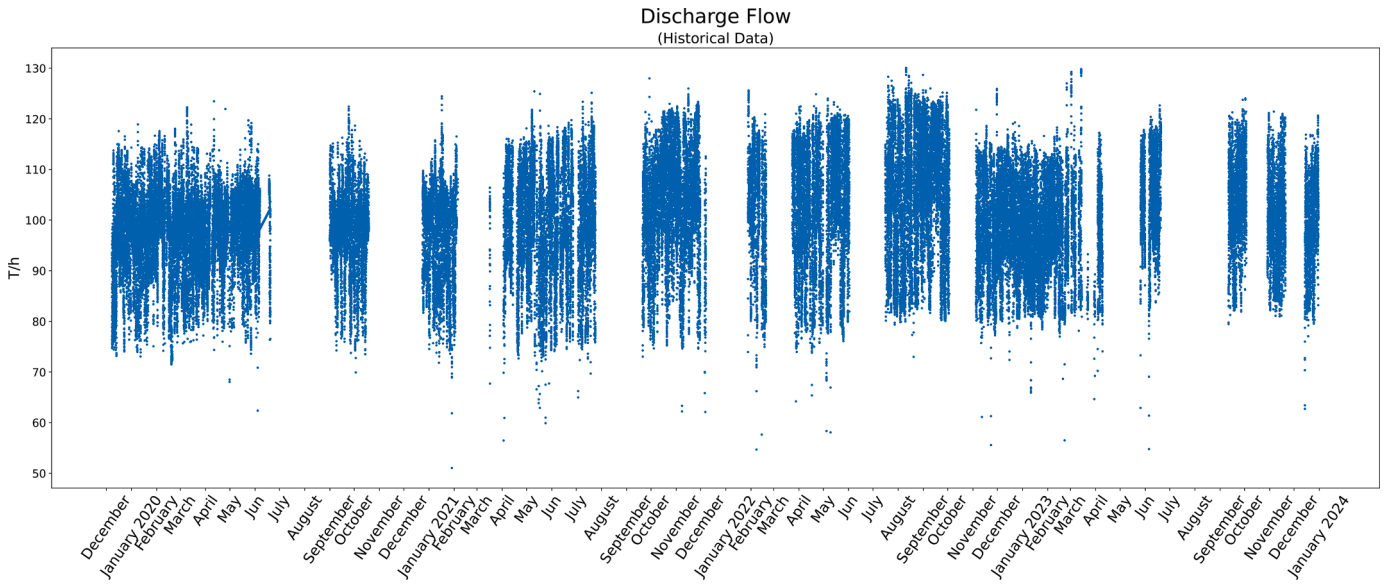

Fig. 7. Historical discharge flow data.

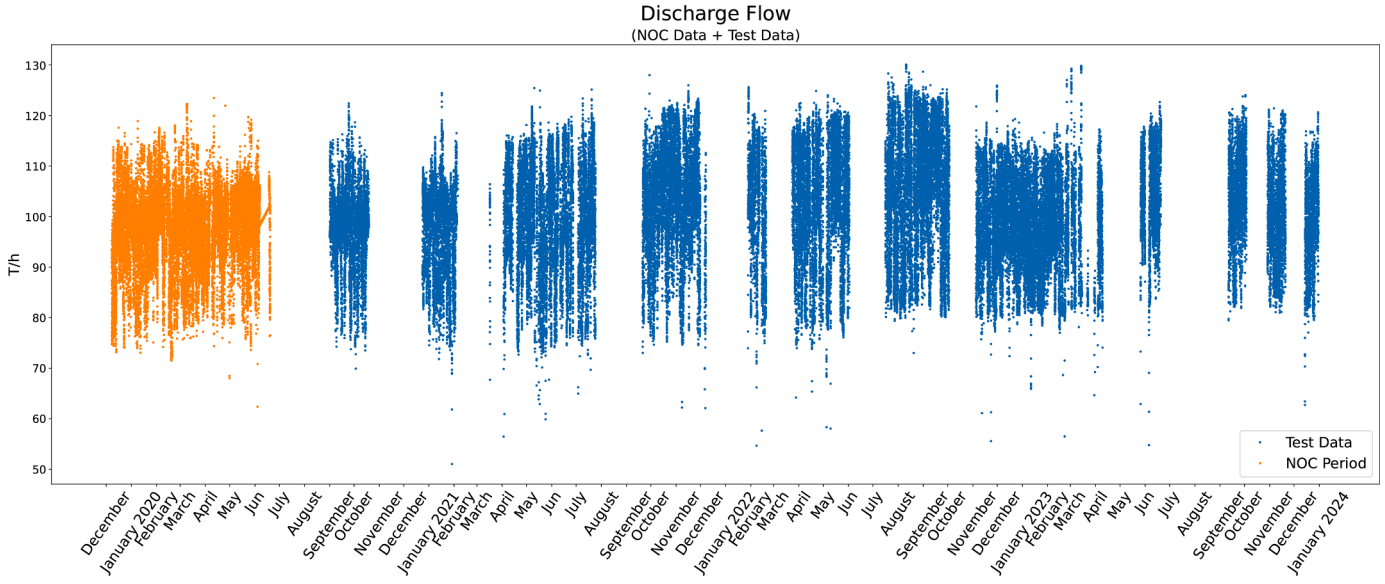

Fig. 8. NOC period identified in the historical discharge flow data.

Table 3
Discharge flow model training results with different ML algorithms.

	LR	kNN	MLP	DT	SVM
RMSE (Training)	1.859	1.451	1.420	1.438	1.464
RMSE (Validation)	1.849	1.457	1.442	1.486	1.459

are as follows: 0.55, 0.15, 0.15 and 0.15, respectively (see Fig. 15). It is clearly observed that the weights comply with Eq. (8).

The risk curves associated with all the failure modes considered in the FMEA are illustrated in Figs. 16 and 17, after the entire procedure described above has been applied to each of the models and failure modes.

3.5. Risk curve diagnosis

Following Section 2.5, this section analyses the risk curves associated with each of the failure modes.

Fig. 16 shows that the most significant increase in risk is associated with the failure modes "Worn OPCS Bearing" (red curve) and "Worn PCS Bearing" (purple curve). These curves illustrate a pronounced and persistent increase that commenced in September 2020 and reached a notably elevated risk level. This indicates that a significant problem has occurred, making failure highly probable or even suggesting that it may have already occurred. Upon examination of the workshop data, it was confirmed that a bearing failure was indeed detected in mid-September.

This failure resulted in a notable increase in vibrations in the OPCS bearing, which subsequently propagated to the PCS bearing. These vibrations are also expected to increase the risk of 'Shaft Misalignment' (grey curve).

The risk associated with the wear of the remaining three bearings also increased in September 2020 as a consequence of the OPCS bearing issue, but to a much lesser extent. However, risk increased again in late 2022, coinciding with new rises in the OPCS and PCS bearing risks. This indicated that a failure affecting all the pump's vibrations was either developing or had already occurred, although determining the precise

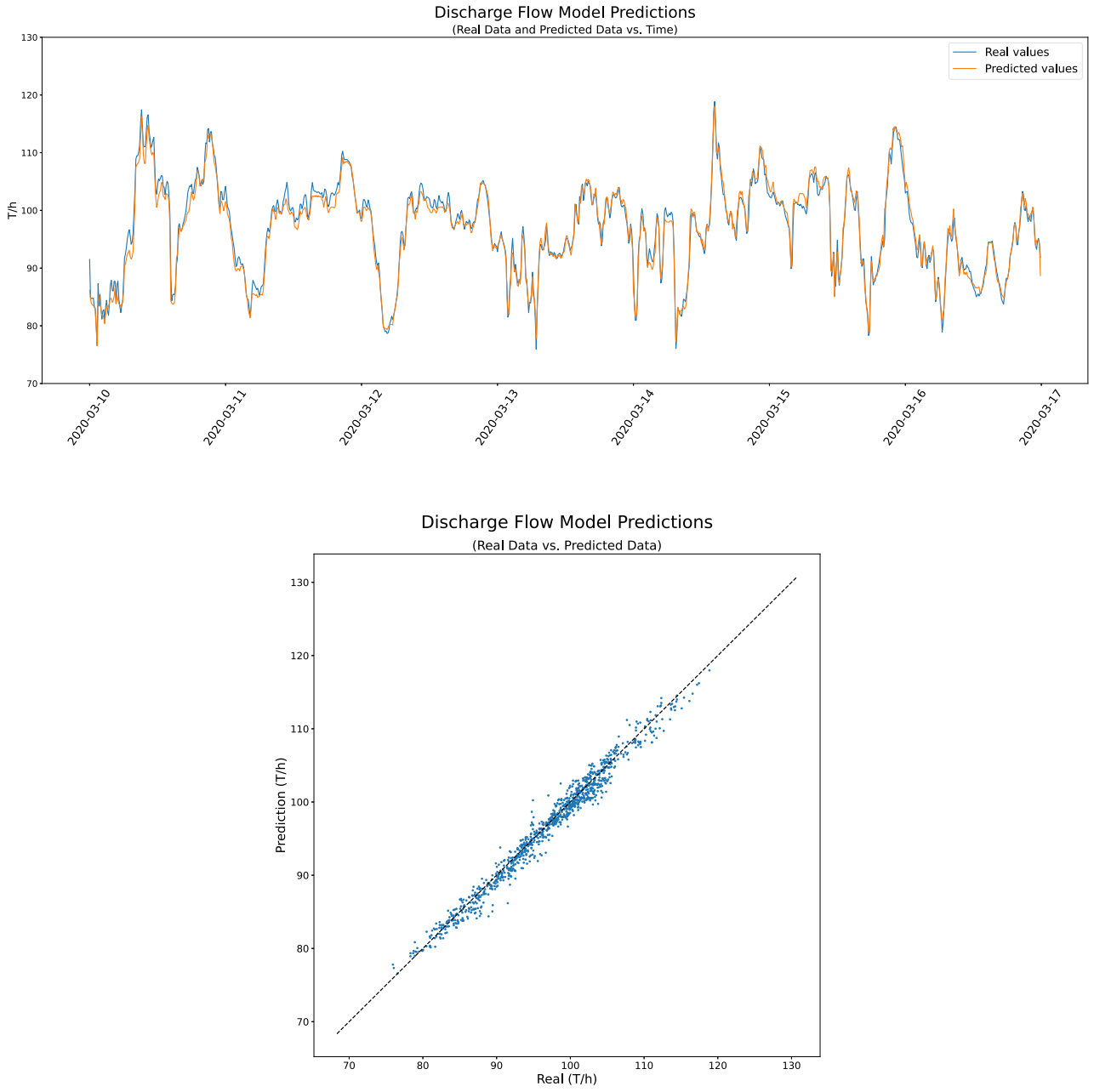

Fig. 9. Example of discharge flow prediction: temporal evolution (top) and prediction vs real (bottom).

Table 4
Discharge flow model hyperparameters.

Discharge Flow Model	
Algorithm	Multi-Layer Perceptron (MLP)
Activation Function	ReLu
Hidden Layers Neurons	12, 14
Learning Rate Init.	0.0056
Learning Rate	Adaptative
Solver	Adam
Alpha	0.0001
Validation fraction	0.2
Max. iterations	10,000
RMSE (Training)	1.4377 T/h
RMSE (Validation)	1.4589 T/h

cause is challenging.

Another curve of interest is the one associated with the risk of "Leak" (pink curve of Fig. 17), which began to rise in August 2021 and has sharply escalated since August 2022. This indicated the presence of a potential leak. Indeed, the workshop records confirmed that a leak was detected and repaired in August 2022. This case highlights the method's ability to identify failures both once they occur and in their early stages, enabling proactive intervention.

The remaining curves are associated with the detected leak, which causes the motor to become overloaded and disrupts its currents. This is evidenced by the increased risk in the blue and yellow curves, respectively. September 2022 marked the point at which the leak reached its peak severity, having previously caused a spike in the risk associated with the "Motor Electrical Failure" failure mode. This current imbalance typically increases motor vibrations, which may explain the rise observed in August 2022 in the bearings less affected by the OPCS failure. However, this remains a hypothesis.

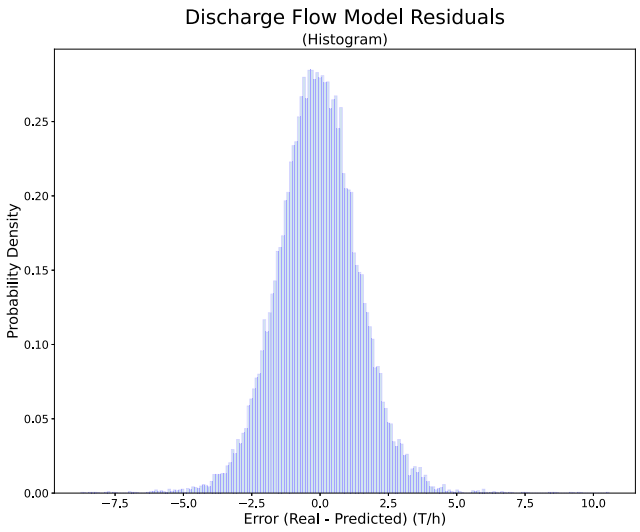

Fig. 10. Distribution of training residuals of the discharge flow model.

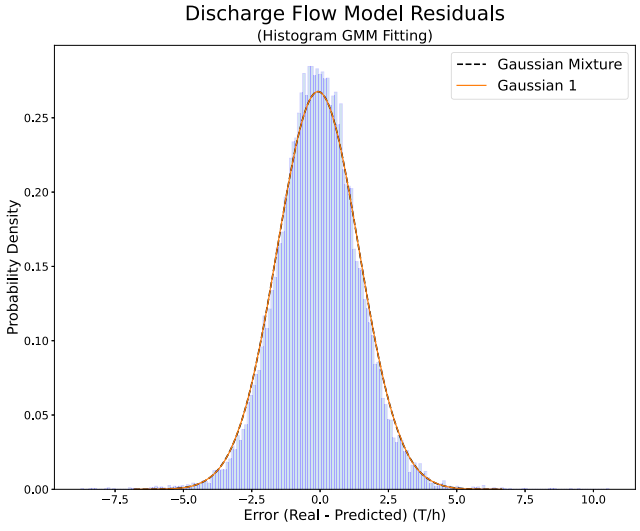

Fig. 11. Fitting of the training residuals distribution of the discharge flow model using GMM.

3.6. Maintenance impact evaluation

Beyond detecting and diagnosing failures, these curves also serve as a platform to overlay maintenance actions over time. This offers two key benefits: comparison of analysis results and evaluation of maintenance effectiveness for each failure mode.

Fig. 18 shows the risk curves together with the dates of preventive maintenance actions (blue vertical lines), which include general checks of temperatures, vibrations, and leaks, oil changes, and corrosion inspections. These actions are scheduled every two months, independently of the pump's condition, and therefore do not serve to verify whether any specific failure mode requires immediate maintenance. Conversely, Fig. 19 shows the risk curves along with the dates of corrective maintenance actions (black vertical lines), which are performed only when a pump component requires repair or replacement. Consequently, these figures allow cross-checking of the obtained results.

In the case under examination, it can be verified that a corrective maintenance action was carried out at the beginning of September 2020. This comprised the replacement of the broken OPCS bearing and the adjustment of the remaining bearing and the shaft. The remaining actions are largely comprised of oil changes, oil refills and minor adjustments to the pump bearings.

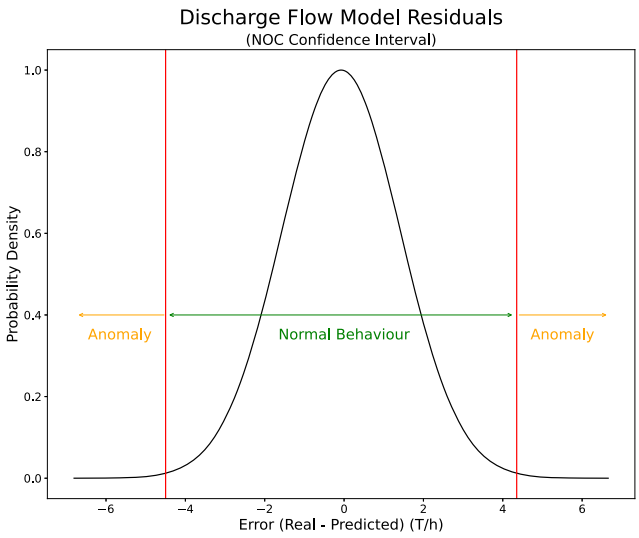

Fig. 12. Characterization of the normal behaviour of the discharge flow by defining the NOC confidence interval.

As anticipated, these curves provide a means of evaluating the efficiency of the actions performed. In addressing this objective, it is necessary to implement Eq. (9) to the dates on which the maintenance actions were conducted.

In order to illustrate these concepts, two specific examples are presented. Firstly, an examination of the red curve, entitled 'Worn OPCS Bearing', and the corrective maintenance action undertaken at the end of November 2021, t_a, will be conducted (Fig. 19). Assuming the initial and final times are defined as $t_{\text{bef}} = t_a - \Delta t$ and $t_{\text{aft}} = t_a + \Delta t$, respectively, with Δt set to one week, the efficiency of the maintenance performed is 73 %. However, if the brown curve ("Worn Thrust Bearing") is considered, the efficiency is 0 %.

A qualitative analysis of the efficiency of the maintenance actions can also be conducted at a glance. It is evident that the last three corrective maintenance actions have had an impact on the failure modes "Worn OPCS Bearing", "Worn PCS Bearing" and "Shaft Misalignment". Prior to these actions, the risk exhibited a positive slope, whereas following them, the slope of the risk curves remains at zero. In any case, it seems that the problem in the OPCS bearing has another origin, since its risk grows gradually and the multiple maintenance procedures performed only have a positive effect temporarily.

We now turn our attention to the preventive maintenance action scheduled for October 2023, t_a, and the pink curve, which represents the "Leak" failure mode (Fig. 18). In this scenario, the efficiency is 100 %, indicating that the leak was rectified subsequent to the execution of the maintenance action. However, this same maintenance action has no discernible effect on the failure modes "Worn OPCS Bearing", "Worn PCS Bearing" and "Shaft Misalignment".

This process was repeated for all maintenance actions and for each of the failure modes, thus allowing the effectiveness of each action to be determined in each case. The results of this study are compiled in Appendix D (Tables 34 and 35).

This analysis, in combination with the diagnosis of the risk curves, results in a series of findings that facilitate the optimisation of maintenance and, consequently, the useful life of the equipment. A thorough examination of the risk curves examined in the preceding section, in conjunction with the corrective and preventive maintenance actions implemented, illuminates the following conclusions:

1. The failure of the OPCS bearing manifests in the associated risk curve in April 2020 (Fig. 16), yet it remains undetected at the plant until 15 September 2020 (see Appendix D), a period of five months.

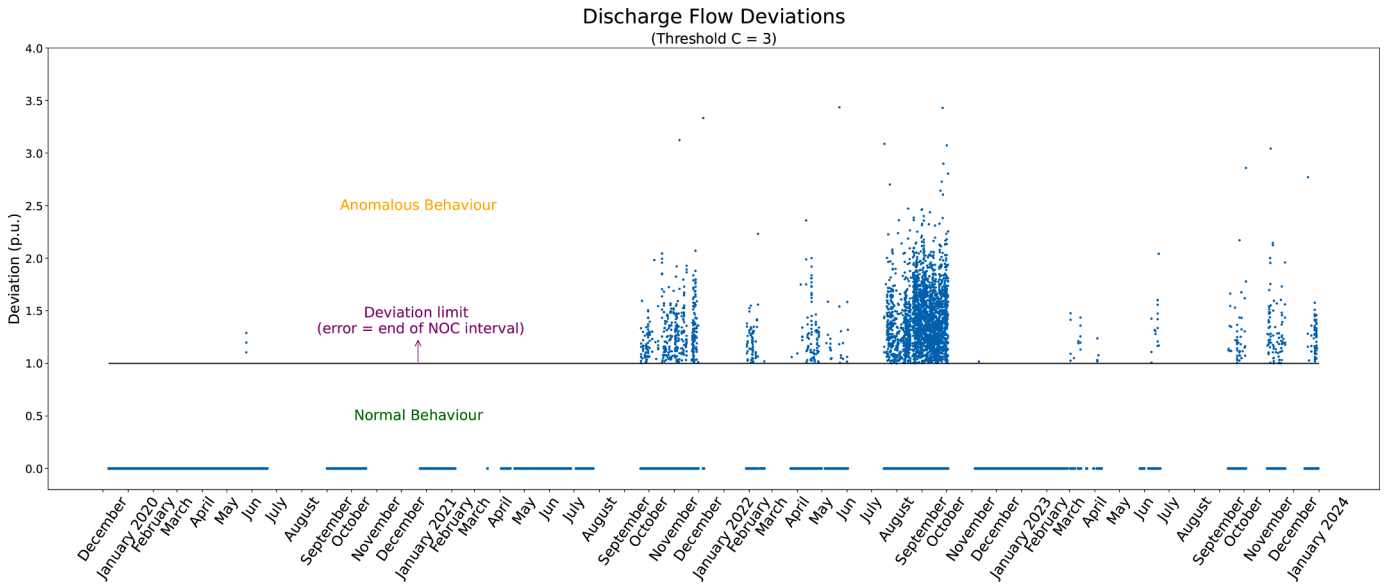

Fig. 13. Discharge flow deviations during the historical data period.

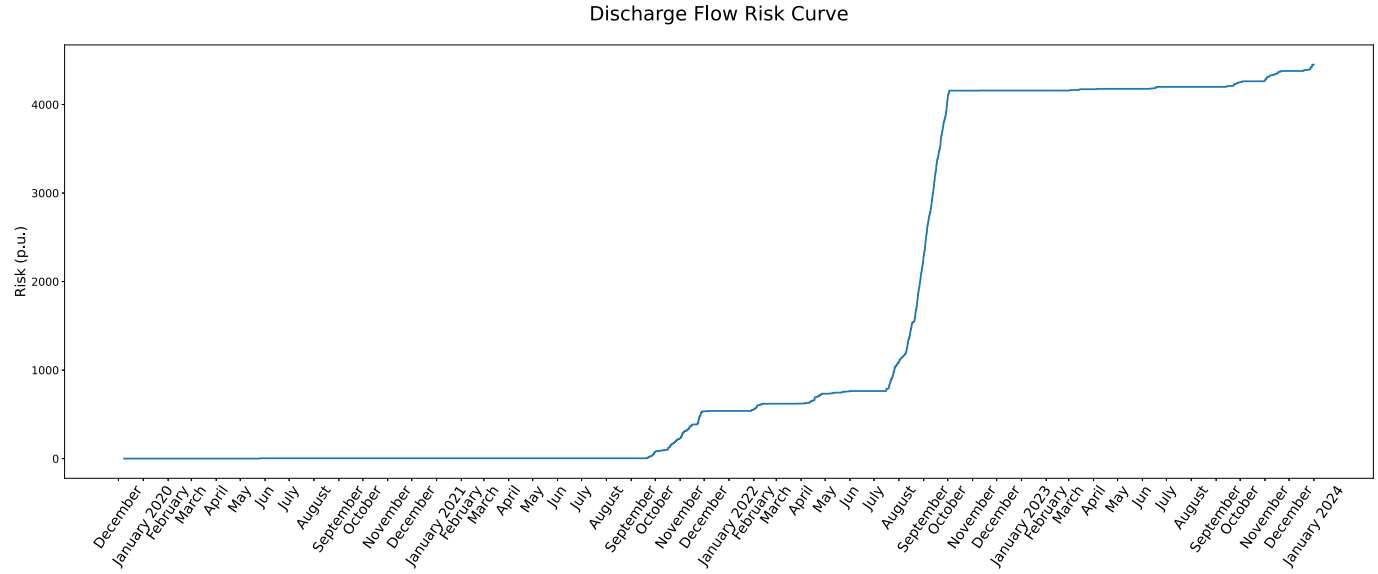

Fig. 14. Constructed risk curve of discharge flow.

2. The "Leak" failure begins to be seen in the associated risk curve in October 2021 (Fig. 17), while the failure is not detected at the plant until February 7, 2022 (see Appendix D), that is, four months later. Furthermore, it is observed that the repair was not effective until preventive maintenance was carried out in October 2022 (Fig. 18).
3. The effectiveness of each of the maintenance actions (see Appendix D) clearly demonstrates that certain actions are more effective than others, and specifically for which failure modes.
4. The mean effectiveness of the preventive maintenance actions for each of the failure modes is approximately 30 % (see Appendix D). Consequently, it is imperative to undertake a comprehensive review of the tasks undertaken, with the objective of optimising their efficacy.

These results highlight the value of the proposed method, which enables early failure detection and could have avoided significant time and cost losses. Furthermore, the quantitative analysis of maintenance actions enables personnel to identify and eliminate ineffective tasks, thereby facilitating effective decision-making and enhancing work efficiency. This ultimately leads to a significant increase in the lifespan of the equipment, resulting in savings in both time and financial resources.

3.7. *Implementation challenges*

The implementation of the proposed methodology in the case study involved several practical challenges, particularly in translating the approach from a conceptual framework into a functional tool for plant personnel. Below, we summarize the main challenges encountered and the strategies used to address them:

1. **User interface and usability**: One of the main challenges was designing an intuitive and accessible tool that could be used efficiently by the plant's maintenance and operations teams. To address this, we developed a dedicated graphical interface that allows real-time visualization of risk curves and their evolution, highlighting

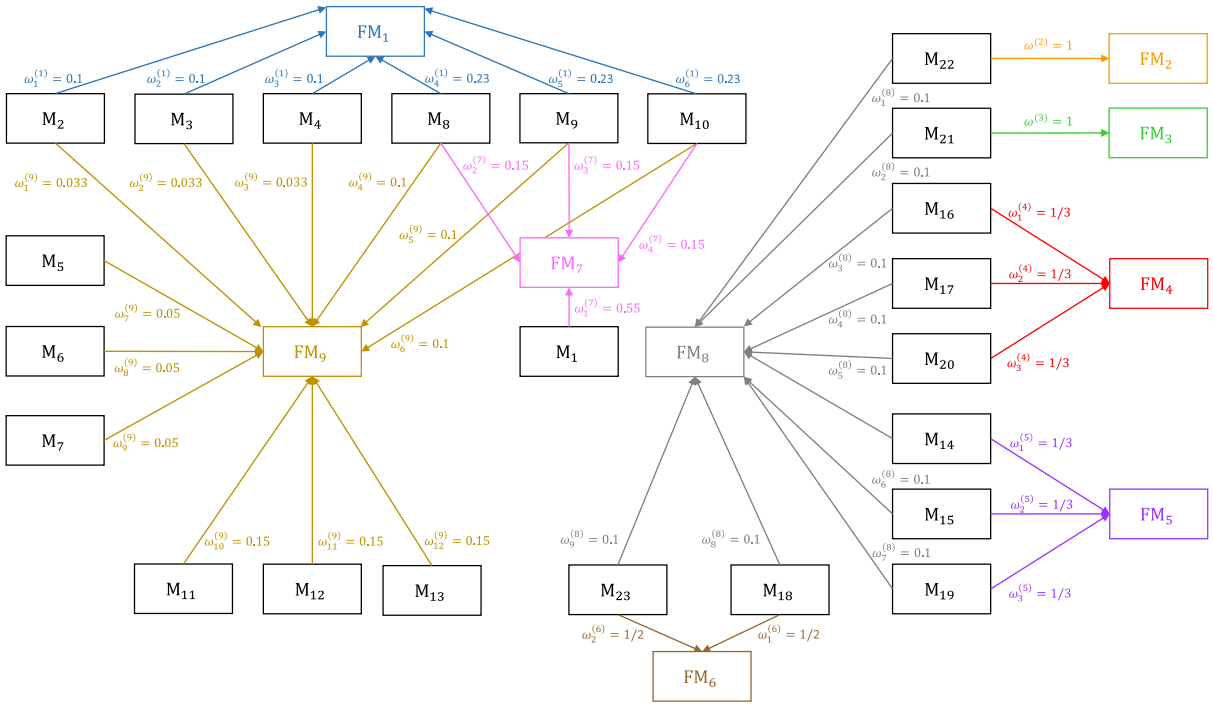

Fig. 15. Relational map between failure modes and equipment models.

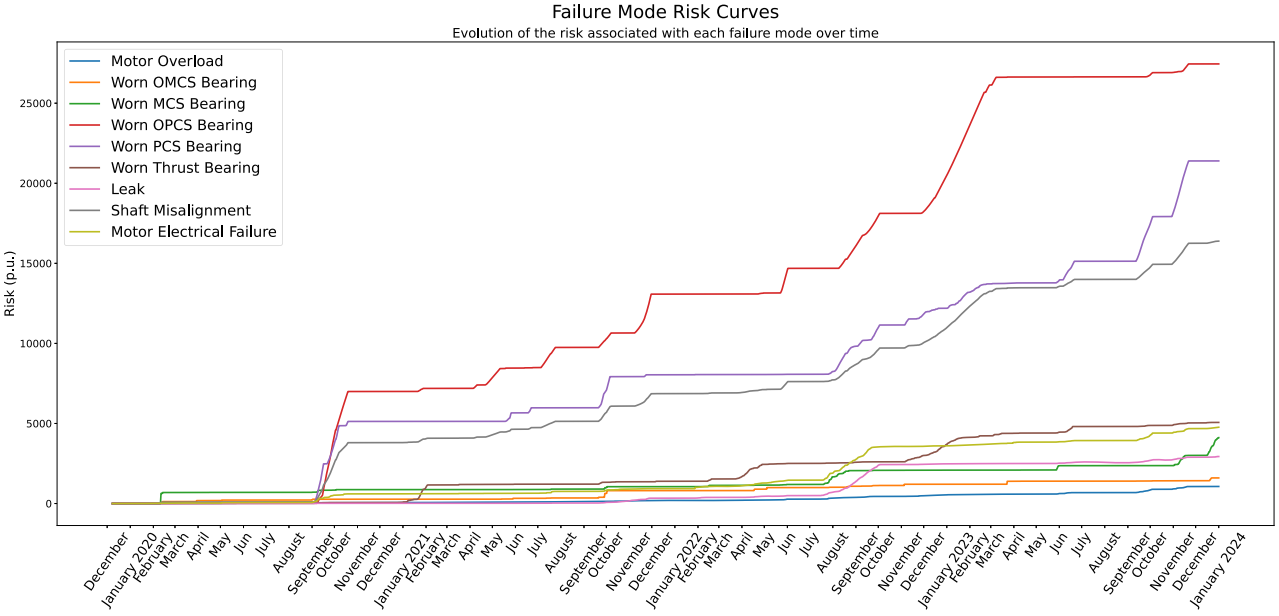

Fig. 16. Risk curves of all pump failure modes analysed.

failure modes and maintenance events in a clear and actionable format.

2. **Generalization to different assets**: Although the case study focuses on a specific feedwater pump, the methodology was implemented in a generic way to ensure adaptability to other monitored assets. This required abstracting core components—such as model configuration, data structure, and risk curve aggregation—to allow flexible application across various types of equipment and failure modes.

Thanks to this modular and asset-agnostic design, applying the methodology to a new system primarily requires defining: (i) the failure modes via FMEA or similar analysis, (ii) the relevant monitored variables for each failure mode, and (iii) the NOC models. Once these elements are established, the rest of the process—including anomaly detection, deviation filtering, risk curve construction, and maintenance evaluation—remains fully applicable without major methodological changes.

However, expert knowledge remains essential to accurately assign monitored variables to failure modes and their relative importance (weights, ω_k). Also, parameters such as the deviation threshold C and the weights (ω_k) themselves may require fine tuning based on experience and historical behaviour of the equipment data.

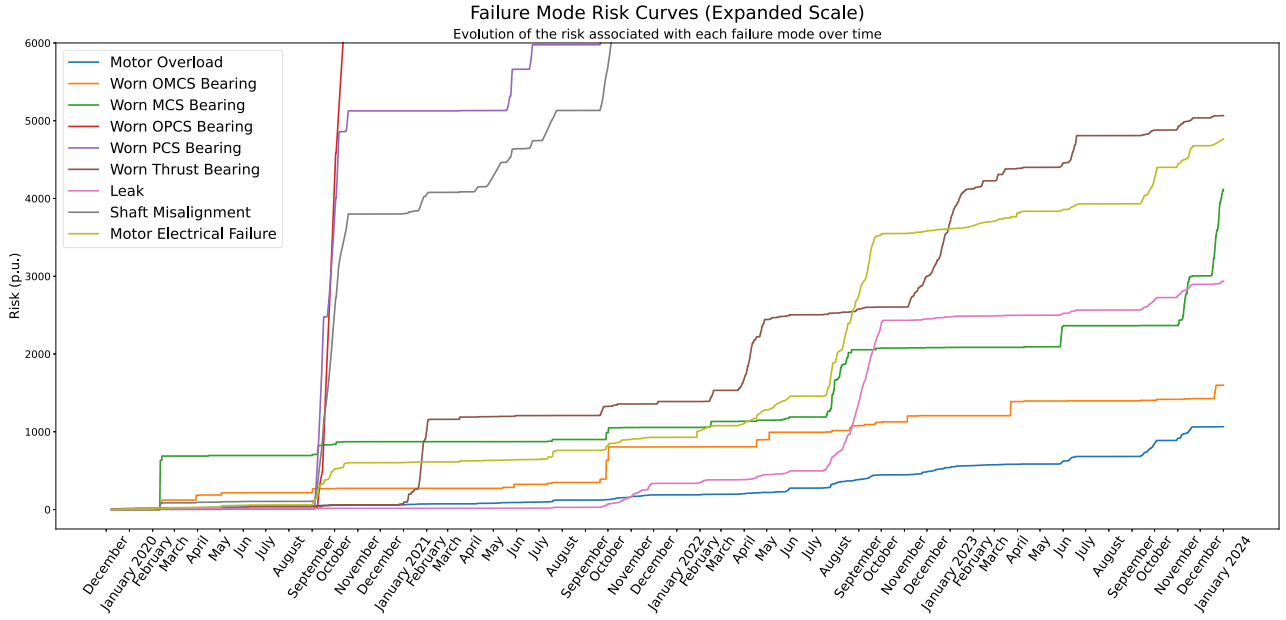

Fig. 17. Risk curves of all pump failure modes analysed (Expanded Scale).

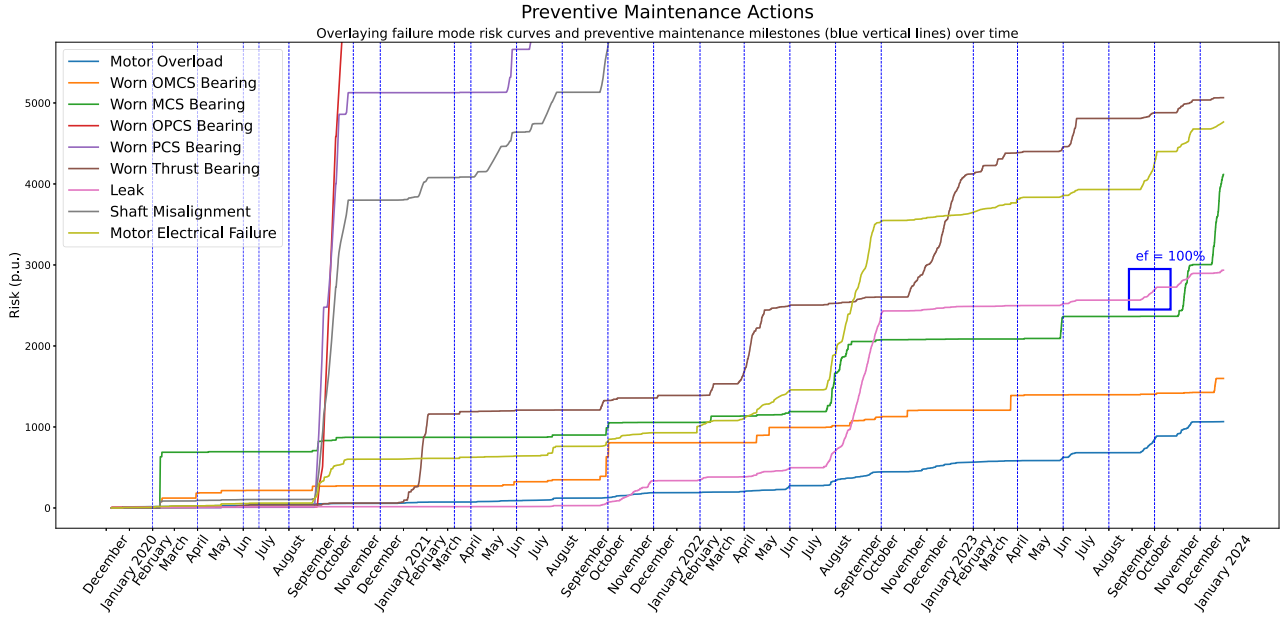

Fig. 18. Overlay of failure mode risk curves and preventive maintenance milestones (blue vertical lines) over time to assess their effectiveness.

1. **Data preprocessing and filtering**: The raw sensor data included transient regimes, noise, and occasional missing values. Careful preprocessing was necessary to isolate valid data under normal operating conditions and to clean the signals before model training. This involved excluding transients, filtering outliers, and aligning timestamps across different signals.
2. **Integration into industrial software platforms**: For full deployment in industrial environments, the methodology can be integrated into CMMS or asset management systems. This requires three main components: (i) a data acquisition layer, capturing real-time sensor data and maintenance logs; (ii) a processing engine, implementing NOC models, deviation detection, risk curve generation, and maintenance effectiveness evaluation; and (iii) a user interface for real-time visualization, alert generation, and reporting. Such integration would enable dynamic, data-driven maintenance directly embedded within existing operational workflows.

These challenges were effectively addressed through collaboration with plant engineers and by incorporating expert knowledge into the configuration of models and thresholds. While these aspects required additional effort, they significantly contributed to the robustness and practical applicability of the proposed methodology.

3.8. *Economic impact estimation*

From an operational and financial perspective, the proposed methodology also offers substantial potential for cost savings by enabling the early detection of failure modes and allowing maintenance to be scheduled proactively, rather than reactively.

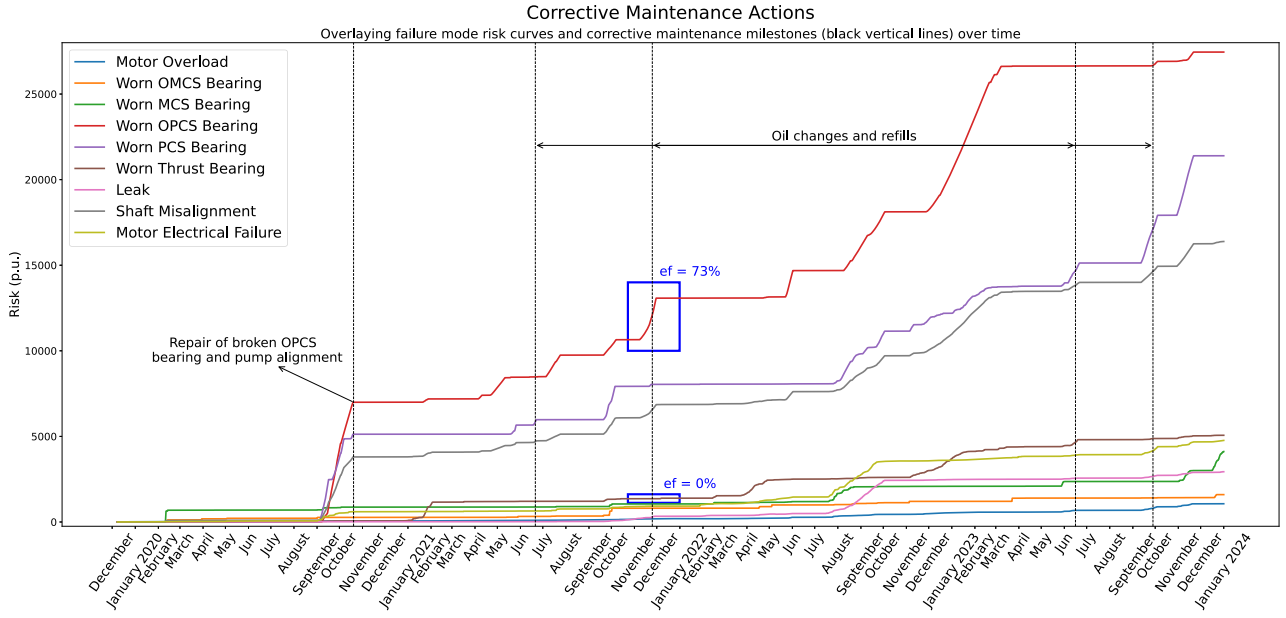

Fig. 19. Overlay of failure mode risk curves and corrective maintenance milestones (black vertical lines) over time to assess their effectiveness.

Based on real data, the cost of a typical preventive maintenance action is estimated in a total cost of 180 € including personnel and material cost.

By contrast, a corrective maintenance action typically involves more resources and production losses. Two scenarios are considered:

1. Optimistic corrective case:
   a. Personnel: 900 € (crew maintenance of 3 members)
   b. Material: 1500 €
   c. Production loss: None, due to the redundancy of another pump, 100 % of capacity
   d. Total: 2400 €
2. Pessimistic corrective case:
   a. Personnel: 1200 € (crew maintenance of 4 members)
   b. Material: 9000 €
   c. Production loss: None, due to the redundancy of another pump, 100 % of capacity
   d. Total: 10,200 €

In the case study, the methodology enabled the early detection of two critical failures, OPCS bearing wear and a leak, four to five months before they were identified by conventional plant operations. If these failures had not been detected early, they would likely have resulted in unplanned corrective maintenance actions. Table 5 summarizes the estimated cost per maintenance action based on the different scenarios.

It is acknowledged that the plant operates with two combined cycles, each supported by four feedwater pumps. According to maintenance records, three corrective maintenance actions were performed annually for each pump before the implementation of our approach. Therefore, it is estimated that, on average, each pump required three corrective maintenance actions per year. Based on these assumptions, the plant's annual maintenance costs are projected to range between €57,600 and €244,800.

Table 5
Estimated cost comparison between preventive and corrective maintenance actions.

Scenario	Corrective Cost	Preventive Cost
Optimistic	2400 €	180 €
Pessimistic	10,200 €	

These results indicate that the methodology not only improves failure anticipation but can also reduce economic losses. Assuming that real cases fall somewhere between these extremes, a weighted average corrective cost of 150,000 € per year is a reasonable estimate of savings for planning purposes.

4. Conclusions

This study introduced a novel methodology to evaluate the effectiveness of maintenance actions in industrial systems through the development and use of 'risk curves' as quantitative failure indicators. By integrating Failure Mode and Effect Analysis (FMEA) with machine learning-based anomaly detection models, the proposed method enables real-time monitoring of equipment health and precise assessment of maintenance actions.

The case study on a feedwater pump in a combined-cycle power plant demonstrated the practical application and effectiveness of this approach. It provided early detection of failures, such as bearing wear and leaks, and allowed a quantified evaluation of the impact of maintenance actions. These findings represent a significant step toward more reliable and informed maintenance strategies in industrial settings.

The key results and insights can be summarized as follows:

1. The methodology successfully detected critical failure modes such as bearing wear and leaks several months before they were identified by conventional operations. These cases emphasize the importance of early failure detection, which can lead to proactive maintenance actions, reduced downtime, and cost savings.
2. A detailed economic analysis (Section 3.8) shows that early detection can reduce the cost of an maintenance action from 180,000–370,000 € (corrective action) to just 180 € (preventive action), depending on the scenario. Preventing 3–5 critical failures per year could translate into annual savings of over 500,000 €.
3. Maintenance actions can be evaluated quantitatively using risk curves. While targeted corrective actions showed up to 73 % risk reduction (e.g., for the OPCS bearing), preventive actions such as inspections or oil changes showed more modest average effectiveness (30 %), highlighting the need to optimize preventive tasks based on actual equipment behaviour.

4. Beyond technical advantages, the methodology improves coordination between operation and maintenance teams by providing clear, real-time visualizations of risk and maintenance actions impact. The risk curves provide clear, quantitative insights into maintenance impacts, fostering a shared understanding of equipment conditions and priorities. Maintenance teams can use this data to justify decisions, allocate resources effectively, and communicate the urgency of specific action. Simultaneously, operation teams gain visibility into maintenance impacts, allowing them to plan production schedules more effectively and minimize disruptions. This decision-making process promotes cooperation and continuous improvement across teams.
5. To the best of our knowledge, no existing methodology integrates failure mode analysis, real-time anomaly detection, and maintenance evaluation into a unified, model-based framework.

While the methodology demonstrated strong performance in the case study, several broader challenges and limitations were identified, particularly during its implementation in an operational environment. These issues are relevant for the generalization and industrial deployment of the proposed framework:

- Expert dependence: Defining failure relationships and model weights still relies on expert input, which introduces subjectivity and limits scalability.
- Sensitivity to noise: Residual-based detection can generate false positives due to signal variability, even with careful pre-processing.
- Behaviour after maintenance: The assumption of a return to "normal" post-maintenance may not hold, requiring adaptive retraining of models.
- Scalability: Applying the method across multiple assets demands flexible, configurable tools for data ingestion, modelling, and visualization.
- User interface and interpretation: The method's effectiveness depends on clear, intuitive visualizations, which remain a challenge across user profiles.

Building on the current findings, several directions for future research are identified to further develop and strengthen the proposed methodology:

- Incorporating maintenance effectiveness into risk: Future versions could make risk curves responsive to past maintenance actions, modelling risk as a dynamic variable.
- Predictive planning from risk evolution: Risk trends could be used to anticipate when maintenance will be needed, complementing or replacing RUL models.
- Data-driven weighting: Model and failure mode weights could be assigned automatically based on historical diagnostic performance.
- Prescriptive integration: Embedding the methodology into systems that recommend actions based on risk, constraints, and resource availability.
- Fleet-wide deployment: Generalizing the method across diverse assets will require scalable architecture and unified dashboards.
- Operationalization into industrial software: To enhance adoption in industrial environments, the methodology could be integrated into CMMS or asset management platforms. This would require (i) a data acquisition layer (sensor data, maintenance logs), (ii) a processing engine (NOC models, risk curve calculation, maintenance evaluation), and (iii) a user interface for real-time visualization, alerts, and maintenance action tracking. Such integration would enable fully data-driven, prescriptive maintenance directly embedded into existing operational workflows.

These research directions aim to enhance the robustness, scalability, and prescriptive value of the methodology, supporting its adoption as a core tool in advanced maintenance management strategies.

The proposed methodology represents a significant advancement in maintenance evaluation, providing both technical and practical contributions to industrial management. By addressing the identified challenges and further optimizing the approach, this framework has the potential to become a cornerstone in predictive and prescriptive maintenance practices. By enabling early failure detection, quantifying maintenance effectiveness, and supporting informed decision-making, this approach helps improve equipment reliability, strengthen collaboration between operations and maintenance teams, reduce costs, and promote sustainable industrial asset management, while remaining readily adaptable to integration within existing industrial maintenance platforms.

Declaration of generative AI and AI-assisted technologies in the writing process

During the preparation of this work the author(s) used ChatGPT in order to improve the quality of writing of certain paragraphs. After using this tool/service, the author(s) reviewed and edited the content as needed and take(s) full responsibility for the content of the publication.

CRediT authorship contribution statement

F. Javier Bellido-Lopez: Writing – review & editing, Writing – original draft, Methodology, Investigation, Formal analysis, Conceptualization. **Miguel A. Sanz-Bobi:** Visualization, Validation, Supervision, Conceptualization. **Antonio Muñoz:** Visualization, Validation, Supervision, Conceptualization. **Daniel Gonzalez-Calvo:** Visualization, Resources. **Tomas Alvarez-Tejedor:** Visualization, Resources.

Declaration of competing interest

The authors declare that they have no known competing financial interests or personal relationships that could have appeared to influence the work reported in this paper.

Acknowledgment

The study has been developed with the scientific and economic support of the ENDESA Chair of Artificial Intelligence Applications to Data-driven Maintenance.

Supplementary materials

Supplementary material associated with this article can be found, in the online version, at doi:10.1016/j.rineng.2025.105809.

Appendix A. FMEA Table

This appendix presents the FMEA conducted for the feedwater pump, including the identified failure modes, their effects, and the associated monitored variables (Table 6):

Table 6
FMEA table.

Failure Mode	Component	Function	Causes	Effects	Detection Methods
Motor overload	Pump motor	Convert electrical energy into mechanical energy, which then powers the pump.	Obstructions in the pump. High water viscosity. Misalignment.	Increased power consumption, vibration and temperature.	Increased motor phase currents.
Motor electrical failure			Short-circuit. Load imbalance. Misalignment.	Unbalanced motor currents.	Distortion of motor phase currents. Increased motor phase temperatures.
Leak	Mechanical seal and tubing	Prevent leakage by creating a barrier between the rotating shaft and the pump housing and transport the pumped fluid, ensuring it reaches the desired destination while maintaining pressure and flow.	Mechanical breakage. Corrosion. Cavitation. Solid particles in the fluid. Impeller/shaft problems.	Fluid leak. Increased power consumption and temperature.	Variation in output flow rate. Variation of motor currents.
Worn OMCS bearing	OMCS bearing	Facilitate smooth, low-friction movement between the different rotating parts of the pump.	Mechanical breakage or wear (corrosion, friction, fatigue). Lack of lubrication.	Increased noise, vibration and temperature. Wear of the bearings themselves and wear and misalignment of the shaft.	Increased bearing vibrations and temperatures.
Worn MCS bearing	MCS bearing				
Worn OPCS bearing	OPCS bearing				
Worn PCS bearing	PCS bearing				
Worn thrust bearing	Thrust bearing				
Shaft misaligned	Pump shaft	Transmit power from the motor to the pump's impeller, enabling the fluid to be propelled through the system.	Mechanical breakage or wear (corrosion, friction, fatigue). Impeller problems (breakage, wear, obstructions). Overload/Obstructions.	Reduction in output pressure and flow. Increased noise, vibration and temperature. Hydraulic instability. Wear of the shaft itself and other components (bearings, seal, etc.).	Increased vibrations and temperatures of the bearings (especially in the misalignment zone). Distortion of motor phase currents. Variations in discharge pressure, flow rate and/or temperature.

Appendix B. Pump variables description

This appendix compiles the description of all the monitored pump variables (Table 7):

Table 7
Description of the pump variables.

Variable	Description	Units
Discharge valve position	Position of the valve that regulates the discharge flow	–
Aspiration pressure	Pressure at the pump inlet	bar
Discharge pressure	Pressure at the pump outlet	bar
Discharge flow rate	Flow at the pump outlet	T/h
Discharge temp.	Temperature at the pump outlet	°C
Phase R current	Pump motor phase R current	A
Phase S current	Pump motor phase S current	A
Phase T current	Pump motor phase T current	A
Average motor current	Average of the three motor currents	A
Phase R temp.	Pump motor phase R temperature	°C
Phase S temp.	Pump motor phase S temperature	°C
Phase T temp.	Pump motor phase T temperature	°C
PCS bear disp. Dir1	Displacement in direction 1 of the Pump Coupling Side bearing	umpp
PCS bear disp. Dir2	Displacement in direction 2 of the Pump Coupling Side bearing	umpp
OPCS bear disp. Dir1	Displacement in direction 1 of the Opposite Pump Coupling Side bearing	umpp
OPCS bear disp. Dir2	Displacement in direction 2 of the Opposite Pump Coupling Side bearing	umpp
Thrust bear vibration	Thrust bearing vibration speed	mm/s
PCS bear temp.	Temperature of the Pump Coupling Side bearing	°C
OPCS bear temp.	Temperature of the Opposite Pump Coupling Side bearing	°C
MCS bear temp.	Temperature of the Motor Coupling Side bearing	°C
OMCS bear temp.	Temperature of the Opposite Motor Coupling Side bearing	°C
Thrust bear temp.	Thrust bearing temperature	°C
Gas turbine power	Combined cycle gas turbine power	MW
Steam turbine power	Combined cycle steam turbine power	MW
Operation mode	Indicator of whether the combined cycle functions in 1 × 1 or 2 × 1 mode	–

Appendix C. NOC models' definition

The following appendix enumerates all defined NOC models of the pump (Tables 8, 9, 10, 11, 12, 13, 14, 15, 16, 17, 18, 19, 20, 21, 22, 23, 24, 25, 26, 27, 28, 29, 30, 31, 32 and 33): mp:

Table 8
Discharge flow model hyperparameters.

Discharge Flow Model	
Algorithm	Multi-Layer Perceptron (MLP)
Activation Function	ReLu
Hidden Layers Neurons	12, 14
Learning Rate Init.	0.0056
Learning Rate	Adaptative
Solver	Adam
Alpha	0.0001
Validation fraction	0.2
Max. iterations	10,000
RMSE (Training)	1.4377 T/h
RMSE (Validation)	1.4589 T/h

Table 9
Discharge pressure model hyperparameters.

Discharge Pressure Model	
Algorithm	Multi-Layer Perceptron (MLP)
Activation Function	ReLu
Hidden Layers Neurons	11, 13, 3, 10
Learning Rate Init.	0.0001
Learning Rate	Constant
Solver	SGD
Alpha	0.0001
Validation fraction	0.2
Max. iterations	10,000
RMSE (Training)	0.4295 bar
RMSE (Validation)	0.4368 bar

Table 10
Discharge temp. model hyperparameters.

Discharge Temp. Model	
Algorithm	Multi-Layer Perceptron (MLP)
Activation Function	ReLu
Hidden Layers Neurons	14, 16, 3
Learning Rate Init.	0.0001
Learning Rate	Constant
Solver	SGD
Alpha	0.00005
Validation fraction	0.2
Max. iterations	10,000
RMSE (Training)	0.1263 °C
RMSE (Validation)	0.1220 °C

Table 11
Discharge pressure-flow model hyperparameters.

Discharge Pressure-Flow Model	
Algorithm	Multi-Layer Perceptron (MLP)
Activation Function	ReLu
Hidden Layers Neurons	15, 12, 6, 12
Learning Rate Init.	0.0001
Learning Rate	Adaptative
Solver	SGD
Alpha	0.0001
Validation fraction	0.2

(*continued on next page*)

Table 11 (*continued*)

Discharge Pressure-Flow Model	
Algorithm	Multi-Layer Perceptron (MLP)
Max. iterations	10,000
RMSE (Training)	0.2855 bar
RMSE (Validation)	0.2779 bar

Table 12
Current phase R model hyperparameters.

Current Phase R Model	
Algorithm	k-Nearest Neighbors (kNN)
Neighbors Number	35
RMSE (Training)	0.5820 A
RMSE (Validation)	0.6030 A

Table 13
Current phase S model hyperparameters.

Current Phase S Model	
Algorithm	k-Nearest Neighbors (kNN)
Neighbors Number	56
RMSE (Training)	0.5498 A
RMSE (Validation)	0.5509 A

Table 14
Current phase T model hyperparameters.

Current Phase T Model	
Algorithm	k-Nearest Neighbors (kNN)
Neighbors Number	19
RMSE (Training)	0.5618 A
RMSE (Validation)	0.5801 A

Table 15
Current phase R power model hyperparameters.

Current Phase R Power Model	
Algorithm	Multi-Layer Perceptron (MLP)
Activation Function	ReLu
Hidden Layers Neurons	16
Learning Rate Init.	0.0067
Learning Rate	Adaptative
Solver	SGD
Alpha	0.0001
Validation fraction	0.2
Max. iterations	10,000
RMSE (Training)	1.1299 A
RMSE (Validation)	1.1465 A

Table 16
Current phase S power model hyperparameters.

Current Phase S Power Model	
Algorithm	Multi-Layer Perceptron (MLP)
Activation Function	tanh
Hidden Layers Neurons	7, 3, 3

(*continued on next page*)

Table 16 (*continued*)

Current Phase S Power Model	
Algorithm	Multi-Layer Perceptron (MLP)
Learning Rate Init.	0.0045
Learning Rate	Constant
Solver	Adam
Alpha	0.00005
Validation fraction	0.2
Max. iterations	10,000
RMSE (Training)	1.2345 A
RMSE (Validation)	1.2150 A

Table 17
Current phase T power model hyperparameters.

Current Phase T Power Model	
Algorithm	Multi-Layer Perceptron (MLP)
Activation Function	tanh
Hidden Layers Neurons	4, 4, 16, 6
Learning Rate Init.	0.0078
Learning Rate	Adaptative
Solver	Adam
Alpha	0.0001
Validation fraction	0.2
Max. iterations	10,000
RMSE (Training)	1.1254 A
RMSE (Validation)	1.1385 A

Table 18
Temp phase R model hyperparameters.

Temp. Phase R Model	
Algorithm	Linear Regression
RMSE (Training)	0.0377 °C
RMSE (Validation)	0.0373 °C

Table 19
Temp phase S model hyperparameters.

Temp. Phase S Model	
Algorithm	Linear Regression
RMSE (Training)	0.0321 °C
RMSE (Validation)	0.0316 °C

Table 20
Temp phase T model hyperparameters.

Temp. Phase T Model	
Algorithm	Linear Regression
RMSE (Training)	0.0395 °C
RMSE (Validation)	0.0400 °C

Table 21
Temp. phase R power model hyperparameters.

Temp. Phase R Power Model	
Algorithm	Multi-Layer Perceptron (MLP)
Activation Function	tanh
Hidden Layers Neurons	15
Learning Rate Init.	0.0067
Learning Rate	Adaptative
Solver	SGD
Alpha	0.00005
Validation fraction	0.2
Max. iterations	10,000
RMSE (Training)	1.9841 °C
RMSE (Validation)	1.9534 °C

Table 22
Temp. phase S power model hyperparameters.

Temp. Phase S Power Model	
Algorithm	Multi-Layer Perceptron (MLP)
Activation Function	tanh
Hidden Layers Neurons	11
Learning Rate Init.	0.0089
Learning Rate	Constant
Solver	Adam
Alpha	0.00005
Validation fraction	0.2
Max. iterations	10,000
RMSE (Training)	1.9748 °C
RMSE (Validation)	1.9828 °C

Table 23
Current phase T power model hyperparameters.

Temp. Phase T Power Model	
Algorithm	Multi-Layer Perceptron (MLP)
Activation Function	ReLu
Hidden Layers Neurons	14, 15, 13, 13
Learning Rate Init.	0.0001
Learning Rate	Constant
Solver	SGD
Alpha	0.00005
Validation fraction	0.2
Max. iterations	10,000
RMSE (Training)	1.9197 °C
RMSE (Validation)	1.9672 °C

Table 24
Disp. Dir1 bear PCS model hyperparameters.

Disp. Dir1 Bear PCS Model	
Algorithm	Multi-Layer Perceptron (MLP)
Activation Function	tanh
Hidden Layers Neurons	11, 7, 16
Learning Rate Init.	0.0034
Learning Rate	Constant
Solver	SGD
Alpha	0.0000
Validation fraction	0.2
Max. iterations	10,000
RMSE (Training)	3.4098 umpp
RMSE (Validation)	3.5005 umpp

Table 25
Disp. Dir2 bear PCS model hyperparameters.

Disp. Dir2 Bear PCS Model	
Algorithm	Multi-Layer Perceptron (MLP)
Activation Function	ReLu
Hidden Layers Neurons	14, 11, 11
Learning Rate Init.	0.0056
Learning Rate	Adaptative
Solver	SGD
Alpha	0.0000
Validation fraction	0.2
Max. iterations	10,000
RMSE (Training)	5.2041 umpp
RMSE (Validation)	5.0698 umpp

Table 26
Disp. Dir1 bear OPCS model hyperparameters.

Disp. Dir1 Bear OPCS Model	
Algorithm	Multi-Layer Perceptron (MLP)
Activation Function	ReLu
Hidden Layers Neurons	14, 5, 16
Learning Rate Init.	0.0023
Learning Rate	Adaptative
Solver	SGD
Alpha	0.0000
Validation fraction	0.2
Max. iterations	10,000
RMSE (Training)	1.6052 umpp
RMSE (Validation)	1.6046 umpp

Table 27
Disp. Dir2 bear OPCS model hyperparameters.

Disp. Dir2 Bear OPCS Model	
Algorithm	Multi-Layer Perceptron (MLP)
Activation Function	ReLu
Hidden Layers Neurons	11, 16, 6, 15
Learning Rate Init.	0.0012
Learning Rate	Adaptative
Solver	SGD
Alpha	0.00005
Validation fraction	0.2
Max. iterations	10,000
RMSE (Training)	3.3349 umpp
RMSE (Validation)	3.1802 umpp

Table 28
Vib. thrust bear model hyperparameters.

Vib. Thrust Bear Model	
Algorithm	Multi-Layer Perceptron (MLP)
Activation Function	tanh
Hidden Layers Neurons	14, 12, 14, 2
Learning Rate Init.	0.0056
Learning Rate	Constant
Solver	Adam
Alpha	0.00005
Validation fraction	0.2
Max. iterations	10,000
RMSE (Training)	0.0502 mm/s
RMSE (Validation)	0.0491 mm/s

Table 29
Temp. bear PCS model hyperparameters.

Temp. Bear PCS Model	
Algorithm	Multi-Layer Perceptron (MLP)
Activation Function	tanh
Hidden Layers Neurons	11, 6, 15
Learning Rate Init	0.0056
Learning Rate	Constant
Solver	Adam
Alpha	0.0001
Validation fraction	0.2
Max. iterations	10,000
RMSE (Training)	0.6953 °C
RMSE (Validation)	0.6880 °C

Table 30
Temp. bear OPCS model hyperparameters.

Temp. Bear OPCS Model	
Algorithm	Multi-Layer Perceptron (MLP)
Activation Function	tanh
Hidden Layers Neurons	13, 1, 16, 10
Learning Rate Init	0.0034
Learning Rate	Constant
Solver	Adam
Alpha	0.0001
Validation fraction	0.2
Max. iterations	10,000
RMSE (Training)	0.7654 °C
RMSE (Validation)	0.7711 °C

Table 31
Temp. bear MCS model hyperparameters.

Temp. Bear MCS Model	
Algorithm	Multi-Layer Perceptron (MLP)
Activation Function	ReLu
Hidden Layers Neurons	15, 10, 3
Learning Rate Init	0.0067
Learning Rate	Constant
Solver	Adam
Alpha	0.00005
Validation fraction	0.2
Max. iterations	10,000
RMSE (Training)	0.5886 °C
RMSE (Validation)	0.6307 °C

Table 32
Temp. bear OMCS model hyperparameters.

Temp. Bear OMCS Model	
Algorithm	Multi-Layer Perceptron (MLP)
Activation Function	tanh
Hidden Layers Neurons	8, 7, 11
Learning Rate Init	0.0056
Learning Rate	Constant
Solver	Adam
Alpha	0.0001
Validation fraction	0.2
Max. iterations	10,000
RMSE (Training)	0.7747 °C
RMSE (Validation)	0.7813 °C

Table 33
Temp. bear thrust model hyperparameters.

Temp. Bear Thrust Model	
Algorithm	Multi-Layer Perceptron (MLP)
Activation Function	tanh
Hidden Layers Neurons	16, 13, 6, 14
Learning Rate Init	0.0056
Learning Rate	Constant
Solver	Adam
Alpha	0.0001
Validation fraction	0.2
Max. iterations	10,000
RMSE (Training)	1.6368 °C
RMSE (Validation)	1.6734 °C

Appendix C. Effectiveness of maintenance actions

The contents of this appendix are comprised of the results obtained from measuring the effectiveness of all maintenance actions performed on the pump throughout the historical data period (Tables 34, 35):

Table 34
Maintenance effectiveness of corrective maintenance actions (%).

Action	**Date**	**Motor Overload**	**Worn OMCS Bearing**	**Worn MCS Bearing**	**Worn OPCS Bearing**	**Worn PCS Bearing**	**Worn Thrust Bearing**	**Leak**	**Shaft Misalignment**	**Motor Electrical Failure**
Shaft Alignment Oil Change (OPCS and PCS) Bearing Part Change (OPCS)	15/09/2020	50.43	94.08	39.64	0.00	22.95	44.81	100.00	0.00	20.52
Shaft Alignment	25/05/2021	0.00	100.00	100.00	27.77	64.96	0.00	100.00	52.08	0.00
Oil Replacement (All)	21/06/2021	44.59	0.00	100.00	0.00	41.81	50.32	0.00	0.00	0.00
Lubrication System Repair (All)	05/10/2021	0.00	100.00	22.88	51.10	88.77	82.67	0.00	78.15	90.76
Oil Replacement (All)	25/11/2021	78.23	0.00	100.00	44.60	100.00	0.00	43.33	56.80	78.50
Leak Repair	07/02/2022	85.54	97.00	0.00	0.00	100.00	99.01	42.94	0.00	48.05
Oil Replacement (All)	16/06/2023	87.45	100.00	100.00	4.47	75.98	28.37	57.62	53.90	0.23
Oil Replacement (PCS)	28/09/2023	26.00	0.00	100.00	42.12	57.83	6.77	39.47	50.34	21.44
Full Intervention	02/12/2023	98.78	100.00	71.72	100.00	100.00	7.93	100.00	96.34	66.12

Table 35
Maintenance effectiveness of preventive maintenance actions (%).

Date	**Motor Overload**	**Worn OMCS Bearing**	**Worn MCS Bearing**	**Worn OPCS Bearing**	Worn PCS Bearing	**Worn Thrust Bearing**	**Leak**	**Shaft Misalignment**	**Motor Electrical Failure**
01/02/2020	30.01	0.00	0.00	0.00	0.00	0.00	41.76	0.00	0.00
01/04/2020	38.80	73.29	83.46	0.00	0.00	31.45	0.00	0.00	0.00
01/06/2020	0.00	32.10	0.00	100.00	100.00	100.00	0.00	97.68	0.00
22/06/2020	100.00	100.00	100.00	0.00	0.00	0.00	100.00	100.00	100.00
01/08/2020	0.00	0.00	0.00	0.00	0.00	0.00	0.00	0.00	0.00
01/10/2020	2.48	64.18	18.52	0.00	0.00	32.19	100.00	0.00	34.01
26/10/2020	100.00	100.00	100.00	100.00	100.00	100.00	0.00	100.00	100.00
01/12/2020	0.00	0.00	0.00	0.00	0.00	0.00	0.00	0.00	0.00

(*continued on next page*)

Table 35 (*continued*)

Date	Motor Overload	Worn OMCS Bearing	Worn MCS Bearing	Worn OPCS Bearing	Worn PCS Bearing	Worn Thrust Bearing	Leak	Shaft Misalignment	Motor Electrical Failure
10/03/2021	100.00	0.00	0.00	95.40	0.00	0.00	0.00	90.27	0.00
01/04/2021	0.00	19.54	0.00	0.00	0.00	0.00	0.00	0.00	30.22
01/06/2021	0.00	0.00	0.00	17.51	49.77	0.00	0.00	26.75	0.00
01/08/2021	74.22	15.94	100.00	69.08	0.00	0.00	0.00	18.86	0.00
01/10/2021	0.00	45.65	0.00	0.00	0.00	76.95	0.00	0.00	0.00
01/12/2021	95.98	0.00	100.00	98.26	96.77	0.00	97.30	97.26	47.73
01/02/2022	0.00	95.44	0.00	0.00	93.98	76.33	0.00	0.00	0.00
01/04/2022	0.00	0.00	0.00	0.00	89.44	0.00	0.00	0.00	0.00
01/06/2022	0.00	0.00	0.00	93.23	0.00	43.81	0.00	86.41	14.42
01/08/2022	0.00	0.00	0.00	0.00	0.00	0.00	0.00	0.00	0.00
01/10/2022	73.84	96.22	92.63	29.03	6.19	0.00	97.42	18.52	96.05
01/02/2023	43.47	0.00	82.94	0.00	26.54	51.02	84.16	12.62	0.00
01/04/2023	0.00	55.07	0.00	93.14	85.68	70.37	0.00	88.35	86.16
01/06/2023	0.00	73.97	94.95	0.00	0.00	0.00	0.00	0.00	0.00
01/08/2023	0.00	0.00	0.00	0.00	0.00	68.56	0.00	0.00	0.00
01/10/2023	0.00	0.00	0.00	0.00	10.64	0.00	0.00	0.00	0.00
01/12/2023	94.66	0.00	0.00	78.89	16.70	15.67	73.95	40.68	0.00
Average	**30.14**	**30.86**	**30.90**	**30.98**	**27.03**	**26.65**	**23.78**	**31.10**	**20.34**

Data availability

The data that has been used is confidential.

References

[1] L. Pintelon, A. Parodi-Herz, Maintenance: an evolutionary perspective. Complex System Maintenance Handbook, Springer Series in Reliability Engineering, Springer London, London, 2008, pp. 21–48, https://doi.org/10.1007/978-1-84800-011-7-2.

[2] A.H. Christer, J. Whitelaw, An operational research approach to breakdown maintenance: problem recognition, J. Oper. Res. Soc. 34 (1983) 1041–1052, https://doi.org/10.1057/jors.1983.235.

[3] K.L. Butler, An expert system based framework for an incipient failure detection and predictive maintenance system, in: Proceedings of the International Conference on Intelligent System Application to Power Systems, Orlando, FL, USA, IEEE, 1996, pp. 321–326, https://doi.org/10.1109/ISAP.1996.501092. Presented at the International Conference on Intelligent System Application to Power Systems.

[4] M. Molęda, B. Małysiak-Mrozek, W. Ding, V. Sunderam, D. Mrozek, From corrective to predictive maintenance—A review of maintenance approaches for the power industry, Sensors 23 (2023) 5970, https://doi.org/10.3390/s23135970.

[5] P. Poor, J. Basl, D. Zenisek, Predictive Maintenance 4.0 as next evolution step in industrial maintenance development, in: Proceedings of the International Research Conference on Smart Computing and Systems Engineering (SCSE), Colombo, Sri Lanka, IEEE, 2019, pp. 245–253, https://doi.org/10.23919/SCSE.2019.8842659. Presented at the 2019 International Research Conference on Smart Computing and Systems Engineering (SCSE).

[6] P. Poór, D. Zenísek, J. Basl, Department of Industrial Engineering and Management University of West Bohemia Univerzitní 8, 306 14 Pilsen, Czech Republic, 2019.

[7] A. Ucar, M. Karakose, N. Kırımça, Artificial intelligence for predictive maintenance applications: key components, Trustworth. Future Trends. Appl. Sci. 14 (2024) 898, https://doi.org/10.3390/app14020898.

[8] S. Ochella, M. Shafieeb, Artificial intelligence in prognostic maintenance, in: Proceedings of the 29th European Safety and Reliability Conference (ESREL), Research Publishing Services, 2019, pp. 3424–3431, https://doi.org/10.3850/978-981-11-2724-3_0188-cd. Presented at the Proceedings of the 29th European Safety and Reliability Conference (ESREL).

[9] E. Zio, Prognostics and health management (PHM): where are we and where do we (need to) go in theory and practice, Reliab. Eng. Syst. Saf. 218 (2022) 108119, https://doi.org/10.1016/j.ress.2021.108119.

[10] M. Achouch, M. Dimitrova, K. Ziane, S. Sattarpanah Karganroudi, R. Dhouib, H. Ibrahim, M. Adda, On predictive maintenance in industry 4.0: overview, models, and challenges, Appl. Sci. 12 (2022) 8081, https://doi.org/10.3390/app12168081.

[11] H.-B. Jun, A review on the advanced maintenance approach for achieving the zero-defect manufacturing system, Front. Manuf. Technol. 2 (2022) 920900, https://doi.org/10.3389/fmtec.2022.920900.

[12] M. M. Jasiulewicz-Kaczmarek, K. Antosz, Industry 4.0 technologies for maintenance management – An overview, in: J. Machado, F. Soares, J. Trojanowska, E. Ottaviano, P. Valášek, D. Reddy, E.A. Perondi, Y. Basova (Eds.), Innovations in Mechanical Engineering II, Lecture Notes in Mechanical Engineering, Springer International Publishing, Cham, 2023, pp. 68–79, https://doi.org/10.1007/978-3-031-09382-1-7.

[13] L. Pinciroli, P. Baraldi, E. Zio, Maintenance optimization in industry 4.0, Reliab. Eng. Syst. Saf. 234 (2023) 109204, https://doi.org/10.1016/j.ress.2023.109204.

[14] K.F. Avila Okada, A. Silva De Morais, L.C. Oliveira-Lopes, L. Ribeiro, A survey on fault detection and diagnosis methods, in: Proceedings of the 14th IEEE International Conference on Industry Applications (INDUSCON), São Paulo, Brazil, IEEE, 2021, pp. 1422–1429, https://doi.org/10.1109/INDUSCON51756.2021.9529495. Presented at the 14th IEEE International Conference on Industry Applications (INDUSCON).

[15] P. Kamat, R. Sugandhi, Anomaly detection for predictive maintenance in industry 4.0- A survey, in: Proceedings of the E3S Web Conference 170, 02007, 2020, https://doi.org/10.1051/e3sconf/202017002007.

[16] S. Thudumu, P. Branch, J. Jin, J. Singh, A comprehensive survey of anomaly detection techniques for high dimensional big data, J. Big Data 7 (2020) 42, https://doi.org/10.1186/s40537-020-00320-x.

[17] C. Ferreira, G. Gonçalves, Remaining useful life prediction and challenges: a literature review on the use of machine learning methods, J. Manuf. Syst. 63 (2022) 550–562, https://doi.org/10.1016/j.jmsy.2022.05.010.

[18] J.E. Office, N. Gebraeel, Y. Lei, N. Li, X. Si, E. Zio, Prognostics and remaining useful life prediction of machinery: advances, opportunities and challenges, J. Dyn. Monit. Diagn. (2023) 1–12, https://doi.org/10.37965/jdmd.2023.148.

[19] S. Ramezani, A. Moini, M. Riahi, Prognostics and health management in machinery: a review of methodologies for RUL prediction and roadmap, Int. J. Ind. Eng. 6 (2019) 38–61.

[20] A. Bonci, S. Longhi, G. Nabissi, F. Verdini, Predictive maintenance system using motor current signal analysis for industrial robot, in: Proceedings of the 24th IEEE International Conference on Emerging Technologies and Factory Automation (ETFA), Zaragoza, Spain, IEEE, 2019, pp. 1453–1456, https://doi.org/10.1109/ETFA.2019.8869067. Presented at the 2019 24th IEEE International Conference on Emerging Technologies and Factory Automation (ETFA).
[21] C.-Y. Lin, Y.-M. Hsieh, F.-T. Cheng, H.-C. Huang, M. Adnan, Time series prediction algorithm for intelligent predictive maintenance, IEEE Robot. Autom. Lett. 4 (2019) 2807–2814, https://doi.org/10.1109/LRA.2019.2918684.
[22] S. Ding, P. Zhang, E. Ding, A. Naik, P. Deng, W. Gui, On the application of PCA technique to fault diagnosis, Tsinghua Sci. Technol. 15 (2010) 138–144, https://doi.org/10.1016/S1007-0214(10)70043-2.
[23] R. Tian, L. Liboni, M. Capretz, Anomaly detection with convolutional autoencoder for predictive maintenance, in: Proceedings of the 9th International Conference on Soft Computing & Machine Intelligence (ISCMI), Toronto, ON, Canada, IEEE, 2022, pp. 241–245, https://doi.org/10.1109/ISCMI56532.2022.10068441. Presented at the 2022 9th International Conference on Soft Computing & Machine Intelligence (ISCMI).
[24] J. Wang, L. Zhang, Y. Zheng, K. Wang, Adaptive prognosis of centrifugal pump under variable operating conditions, Mech. Syst. Signal Process. 131 (2019) 576–591, https://doi.org/10.1016/j.ymssp.2019.06.008.
[25] P. Weber, G. Medina-Oliva, C. Simon, B. Iung, Overview on Bayesian networks applications for dependability, risk analysis and maintenance areas, Eng. Appl. Artif. Intell. 25 (2012) 671–682, https://doi.org/10.1016/j.engappai.2010.06.002.
[26] A. Ouadah, L. Zemmouchi-Ghomari, N. Salhi, Selecting an appropriate supervised machine learning algorithm for predictive maintenance, Int. J. Adv. Manuf. Technol. 119 (2022) 4277–4301, https://doi.org/10.1007/s00170-021-08551-9.
[27] G. Qian, J. Liu, A comparative study of deep learning-based fault diagnosis methods for rotating machines in nuclear power plants, Ann. Nucl. Energy 178 (2022) 109334, https://doi.org/10.1016/j.anucene.2022.109334.
[28] A. Widodo, B.-S. Yang, Support vector machine in machine condition monitoring and fault diagnosis, Mech. Syst. Signal Process. 21 (2007) 2560–2574, https://doi.org/10.1016/j.ymssp.2006.12.007.
[29] F. Crawley, 12 - Failure modes and effects analysis (FMEA) and failure modes, effects and criticality analysis (FMECA), in: F. Crawley (Ed.), A Guide to Hazard Identification Methods (Second Edition), Elsevier, 2020, pp. 103–109, https://doi.org/10.1016/B978-0-12-819543-7.00012-4.
[30] Lipol, L.S., Haq, J., 2011. Risk analysis method: FMEA/FMECA in the organizations. 11.
[31] K.R. Aswin, V.R. Renjith, K.R. Akshay, FMECA using fuzzy logic and grey theory: a comparitve case study applied to ammonia storage facility, Int. J. Syst. Assur. Eng. Manag. 13 (2022) 2084–2103, https://doi.org/10.1007/s13198-022-01620-6.
[32] B. Ervural, H.I. Ayaz, A fully data-driven FMEA framework for risk assessment on manufacturing processes using a hybrid approach, Eng. Fail. Anal. 152 (2023) 107525, https://doi.org/10.1016/j.engfailanal.2023.107525.
[33] Z. Wang, R. Wang, W. Deng, Y. Zhao, An integrated approach-based FMECA for risk assessment: application to offshore wind turbine pitch system, Energies 15 (2022) 1858, https://doi.org/10.3390/en15051858.
[34] F.D. Carlo, M.A. Arleo, Imperfect maintenance models, from theory to practice, in: C. Volosencu (Ed.), Proceedings of the System Reliability. InTech, 2017, https://doi.org/10.5772/intechopen.69286.
[35] M. Ghaleb, S. Taghipour, Assessing the impact of maintenance practices on asset's sustainability, Reliab. Eng. Syst. Saf. 228 (2022) 108810, https://doi.org/10.1016/j.ress.2022.108810.
[36] A. Van Horenbeek, L. Pintelon, Development of a maintenance performance measurement framework—using the analytic network process (ANP) for maintenance performance indicator selection, Omega (Westport) 42 (2014) 33–46, https://doi.org/10.1016/j.omega.2013.02.006.
[37] B. El Hajj, F. Schoefs, B. Castanier, T. Yeung, A condition-based deterioration model for the stochastic dependency of corrosion rate and crack propagation in corroded concrete structures, Comput.-Aided Civ. Infrastruct. Eng. 32 (2017) 18–33, https://doi.org/10.1111/mice.12208.
[38] S. Labi, K. Sinha, The effectiveness of maintenance and its impact on capital expenditures, JTRP Tech. Rep. (2003), https://doi.org/10.5703/1288284313331.
[39] M. Memarzadeh, M. Pozzi, Integrated inspection scheduling and maintenance planning for infrastructure systems, Comput.-Aided Civ. Infrastruct. Eng. 31 (2016) 403–415, https://doi.org/10.1111/mice.12178.
[40] Z. Liu, R. Balieu, N. Kringos, Integrating sustainability into pavement maintenance effectiveness evaluation: a systematic review, Transp. Res. Part Transp. Environ. 104 (2022) 103187, https://doi.org/10.1016/j.trd.2022.103187.
[41] M. Alinizzi, S. Chen, S. Labi, A. Kandil, A methodology to account for one-way infrastructure interdependency in preservation activity scheduling, Comput.-Aided Civ. Infrastruct. Eng. 33 (2018) 905–925, https://doi.org/10.1111/mice.12380.
[42] K.G. Papakonstantinou, C.P. Andriotis, M. Shinozuka, POMDP and MOMDP solutions for structural life-cycle cost minimization under partial and mixed observability, Struct. Infrastruct. Eng. 14 (2018) 869–882, https://doi.org/10.1080/15732479.2018.1439973.
[43] S. Thöns, On the value of monitoring information for the structural integrity and risk management, Comput.-Aided Civ. Infrastruct. Eng. 33 (2018) 79–94, https://doi.org/10.1111/mice.12332.
[44] R. Li, Y. Yuan, W. Zhang, Y. Yuan, Unified vision-based methodology for simultaneous concrete defect detection and geolocalization, Comput.-Aided Civ. Infrastruct. Eng. 33 (2018) 527–544, https://doi.org/10.1111/mice.12351.
[45] W. Wang, A. Zhang, K.C.P. Wang, A.F. Braham, S. Qiu, Pavement crack width measurement based on Laplace's equation for continuity and unambiguity, Comput.-Aided Civ. Infrastruct. Eng. 33 (2018) 110–123, https://doi.org/10.1111/mice.12319.
[46] L.Q.M.D. Costa, C.A.V. Cavalcante, A review on the study of maintenance effectiveness, Pesqui. Oper 42 (2022) e263613, https://doi.org/10.1590/0101-7438.2022.042nspe1.00263613.
[47] P. Alavian, Y. Eun, K. Liu, S.M. Meerkov, L. Zhang, The (α, β)-precise estimates of MTBF and MTTR: definition, calculation, and observation time, IEEE Trans. Autom. Sci. Eng. 18 (2021) 1469–1477, https://doi.org/10.1109/TASE.2020.3017134.
[48] P. Sinha, Towards higher maintenance effectiveness, Int. J. Qual. Reliab. Manag. 32 (2015) 754–762, https://doi.org/10.1108/IJQRM-03-2013-0039.
[49] M. Bengtsson, G. Lundström, On the importance of combining "the new" with "the old" – one important prerequisite for maintenance in Industry 4.0, Procedia Manuf. 25 (2018) 118–125, https://doi.org/10.1016/j.promfg.2018.06.065.
[50] Z. Sajaradj, L.N. Huda, S. Sinulingga, The application of reliability centered maintenance (RCM) methods to design maintenance system in manufacturing (Journal Review), IOP Conf. Ser. Mater. Sci. Eng 505 (2019) 012058, https://doi.org/10.1088/1757-899X/505/1/012058.
[51] Singh, D., Suhane, A., 2013. Study of centrifugal pump using failure mode effect and critical analysis based on fuzzy cost estimation: a case Study 4.
[52] Staroswiecki, M., Comtet-Varga, G., 2001. Analytical redundancy relations for fault detection and isolation in algebraic dynamic systems.
[53] R. Isermann, Model-based fault-detection and diagnosis – status and applications, Annu. Rev. Control 29 (2005) 71–85, https://doi.org/10.1016/j.arcontrol.2004.12.002.
[54] F. Calabrese, A. Regattieri, M. Bortolini, F.G. Galizia, Data-driven fault detection and diagnosis: challenges and opportunities in real-world scenarios, Appl. Sci. 12 (2022) 9212, https://doi.org/10.3390/app12189212.
[55] Y. Xu, Y. Sun, J. Wan, X. Liu, Z. Song, Industrial big data for fault diagnosis: taxonomy, review, and applications, IEEE Access. 5 (2017) 17368–17380, https://doi.org/10.1109/ACCESS.2017.2731945.
[56] Y. Zhao, T. Li, X. Zhang, C. Zhang, Artificial intelligence-based fault detection and diagnosis methods for building energy systems: advantages, challenges and the future, Renew. Sustain. Energy Rev. 109 (2019) 85–101, https://doi.org/10.1016/j.rser.2019.04.021.
[57] R. Chambers, Fossil Maintenance Applications Center: Combined-Cycle Combustion-Turbine Segmented-Casing Feedwater Pump Maintenance Guideline (Technical), EPRI (2010).
[58] M.M. Ali, B.K. Paul, K. Ahmed, F.M. Bui, J.M.W. Quinn, M.A. Moni, Heart disease prediction using supervised machine learning algorithms: performance analysis and comparison, Comput. Biol. Med. 136 (2021) 104672, https://doi.org/10.1016/j.compbiomed.2021.104672.
[59] Babcock University, F.Y, O., J.E.T, A., O, A., J. O, H., O, O., J, A., Supervised machine learning algorithms: classification and comparison, Int. J. Comput. Trends Technol. 48 (2017) 128–138, https://doi.org/10.14445/22312803/IJCTT-V48P126.
[60] B. Mahesh, Machine learning algorithms - a review, Int. J. Sci. Res. IJSR 9 (2020) 381–386, https://doi.org/10.21275/ART20203995.
[61] I.H. Sarker, Machine learning: algorithms, real-world applications and research directions, SN Comput. Sci. 2 (2021) 160, https://doi.org/10.1007/s42979-021-00592-x.
[62] A. Jafar, M. Lee, Comparative performance evaluation of state-of-the-art hyperparameter optimization frameworks, Trans. Korean Inst. Electr. Eng. 72 (2023) 607–620, https://doi.org/10.5370/KIEE.2023.72.5.607.
[63] J. Joy, M.P. Selvan, A comprehensive study on the performance of different multi-class classification algorithms and hyperparameter tuning techniques using Optuna, in: Proceedings of the International Conference on Computing, Communication, Security and Intelligent Systems (IC3SIS), 2022, pp. 1–5, https://doi.org/10.1109/IC3SIS54991.2022.9885695. Presented at the 2022 International Conference on Computing, Communication, Security and Intelligent Systems (IC3SIS).
[64] D.C. Montgomery, Introduction to Statistical Quality Control, John Wiley & Sons, 2020.